# Frequency-dependent seismic attenuation in the inner core 1. A viscoelastic interpretation

Xu Li[1] and Vernon F. Cormier

Department of Geology and Geophysics, University of Connecticut, Storrs, USA

Received 28 January 2002; revised 20 July 2002; accepted 19 August 2002; published 21 December 2002.

[1] Using reference source time functions, broadband velocity waveforms of PKIKP in the distance range 150–180° are inverted for a viscoelastic model of inner core attenuation. A mean $Q_\alpha$ at 1 Hz of 307 ± 90 is determined from 345 available PKIKP ray paths. Both global and regional results find a depth-dependent attenuation in the deep inner core, with anisotropic attenuation resolved in regional results. Attenuation is much stronger in the upper 300 km of the inner core. The preferred model of viscoelastic attenuation is frequency dependent, with very weak velocity dispersion. Our data do not resolve any hemispherical differences of attenuation in the deep inner core. *INDEX TERMS:* 8115 Tectonophysics: Core processes (1507); 8124 Tectonophysics: Earth's interior—composition and state (old 8105); 7203 Seismology: Body wave propagation; 7207 Seismology: Core and Mantle; 3210 Mathematical Geophysics: Modeling; *KEYWORDS:* inner core, seismic attention, viscoelasticity

**Citation:** Li, X., and V. F. Cormier, Frequency-dependent seismic attenuation in the inner core, 1, A viscoelastic interpretation, *J. Geophys. Res.*, *107*(B12), 2361, doi:10.1029/2002JB001795, 2002.

## 1. Introduction

### 1.1. History of Previous Studies

[2] Anomalous high attenuation in the inner core was found more than 30 years ago from body wave studies [*Sacks*, 1969]. Its depth-dependence and frequency-dependence, however, have long been in debate.

#### 1.1.1. Depth Dependence

[3] Based on models of a cooling Earth and metallurgical experiments, *Fearn et al.* [1981] proposed that the continuous solidification of iron alloy would lead to a partially molten inner core with a melt fraction decreasing with depth. The existence of depth-dependent seismic attenuation in the inner core may support this model. Previous studies, however, have been unable to consistently resolve such a depth dependence. Analyzing spectra and waveforms of PKP-DF and PKP-BC, *Souriau and Roudil* [1995] preferred a model with $Q_\alpha$ close to 200 just under the inner core boundary (ICB), increasing to 400 $\sim$ 600 in the depth interval 200 $\sim$ 400 km. Using similar data, *Niazi and Johnson* [1992] and *Bhattacharyya et al.* [1993] were unable to resolve a depth dependence of attenuation in the upper inner core.

#### 1.1.2. Frequency Dependence

[4] From normal mode data, *Widmer et al.* [1991] found that the shear attenuation factor $Q_\mu$ in the inner core is about 110. Assuming viscoelastic attenuation in pure shear, this value is much higher than the $Q_\mu$ value ($\sim$30) inferred from PKIKP waves [*Cormier*, 1981; *Doornbos*, 1983]. Because the dominant frequencies of normal mode data and body wave data are about 0.001 Hz and 1 Hz, respectively, this difference may be reconciled by a frequency-dependent attenuation in the inner core. Like the question of depth-dependence, there have not been consistent results in the search for frequency dependence. *Bhattacharyya et al.* [1993] and *Souriau and Roudil* [1995] prefer a frequency independent attenuation in the uppermost few hundred km of inner core. *Doornbos* [1983] and *Cummins and Johnson* [1988], however, argue that the weak dispersion seen in PKIKP waveforms is best fit by a frequency-dependent attenuation. Likewise in a recent preliminary study [*Cormier et al.*, 1998] we also favor a frequency-dependent attenuation model to fit PKIKP waveforms in the range 153–170°.

#### 1.1.3. Anisotropy

[5] With the discovery of elastic anisotropy in the inner core, it has been of interest to determine whether the elastic anisotropy is also associated with an anelastic anisotropy. For some mechanisms of elastic anisotropy, an anisotropic anelasticity is also expected [*Carcione and Cavallini*, 1994]. A few previous observations have called attention to the very low amplitudes of PKIKP waves propagating nearly parallel to the Earth's rotation axis compared to the amplitudes of PKIKP waves propagating perpendicular or obliquely to the rotation axis [*Creager*, 1992; *Song and Helmberger*, 1995]. These observations, however, are too sparse to provide useful constraints on attenuation because they sample different regions and could potentially be explained by effects of lateral heterogeneity along the travel paths. An exception is the study of *Souriau and Romanowicz* [1996] who analyzed PKP-DF/BC amplitude ratios for waves sampling the inner core under western Africa.

#### 1.1.4. Constraints From Mineral Physics

[6] Experimental and theoretical mineral physics provide additional constraints on inner core attenuation. At temperatures between 400°C and 1300°C, *Jackson et al.* [2000]

[1]Now at Earth Resources Laboratory, Department of Earth, Atmospheric, and Planetary Science, Massachusetts Institute of Technology, Cambridge, Massachussetts, USA.


0148-0227/02/2002JB001795$09.00

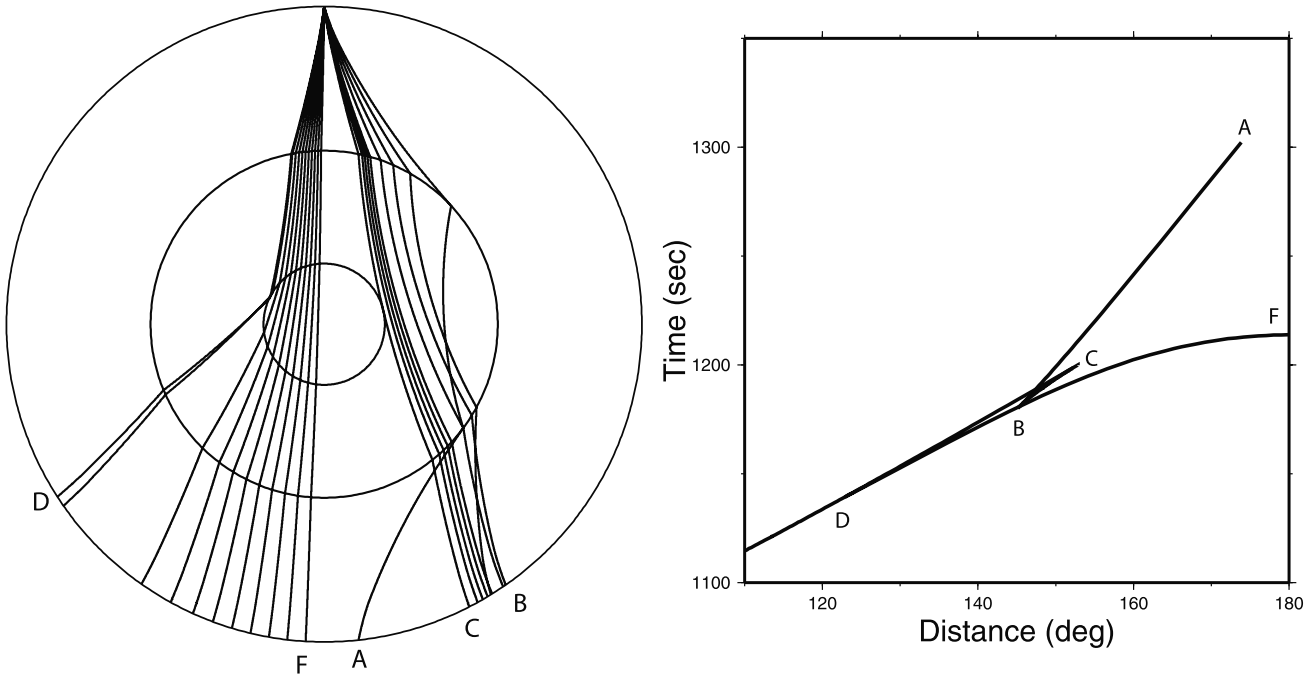


**Figure 1.** Left: ray paths for PKP-AB, -BC, and -DF branches. The BC branch becomes diffracted at ~153°. The AB branch strongly interacts with the lowermost mantle, which may be a region of increased scattering and intrinsic attenuation. Right: travel times for PKP phases as a function of epicentral distance.

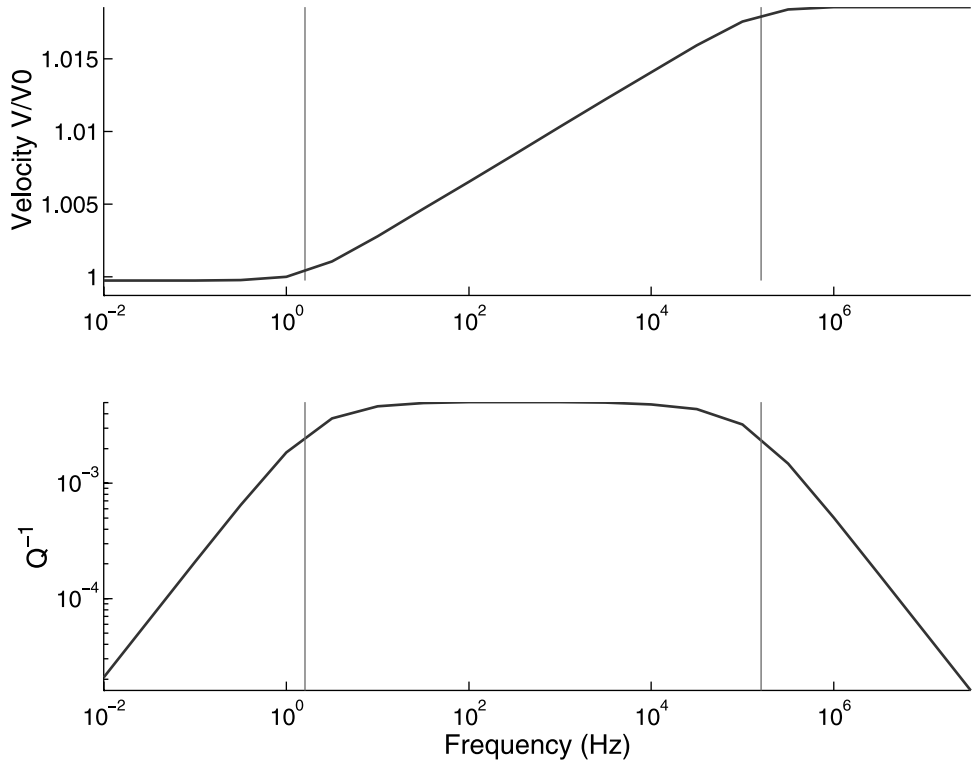


**Figure 2.** The velocity dispersion and relaxation spectrum of an absorption band model with $1/2\pi\tau_1$ = 0.1 Hz, $1/2\pi\tau_2$ = 10,000 Hz, and $Q_m^{-1}$ = 0.005. The two thin lines indicate the low (left) and high (right) frequency corners ($1/2\pi\tau_{1,2}$) of the relaxation spectrum.

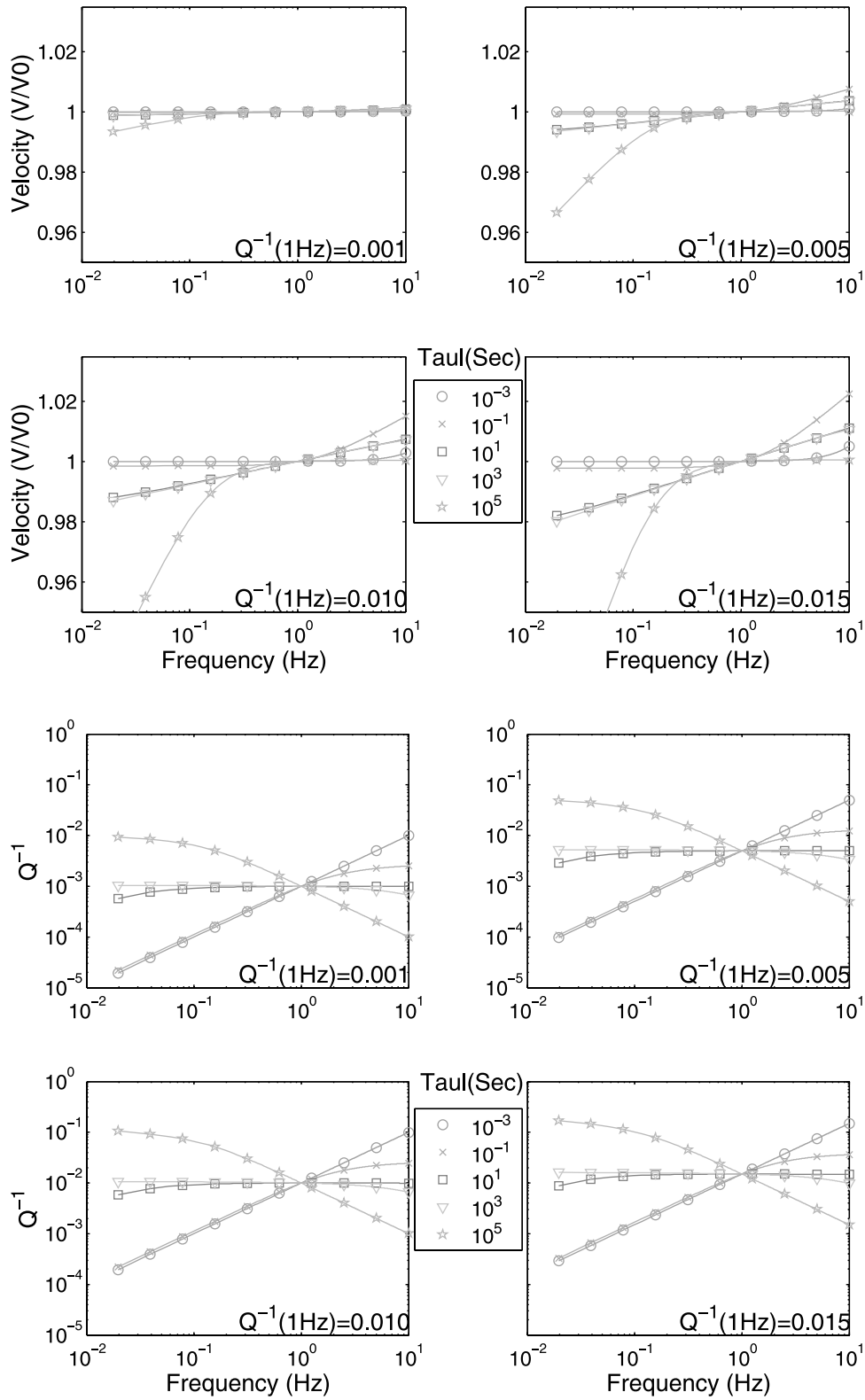


**Figure 3.** Velocity dispersion (a) and relaxation spectrum (b) for four values of $Q^{-1}$ at 1 Hz increasing from $Q^{-1}$(1 Hz) 0.001 (upper left) to 0.015 (lower right). The width of the relaxation spectrum is taken to be constant, with the low frequency corner (see legends) varying from $\tau_1 = 0.003$ s to $10^5$ s.

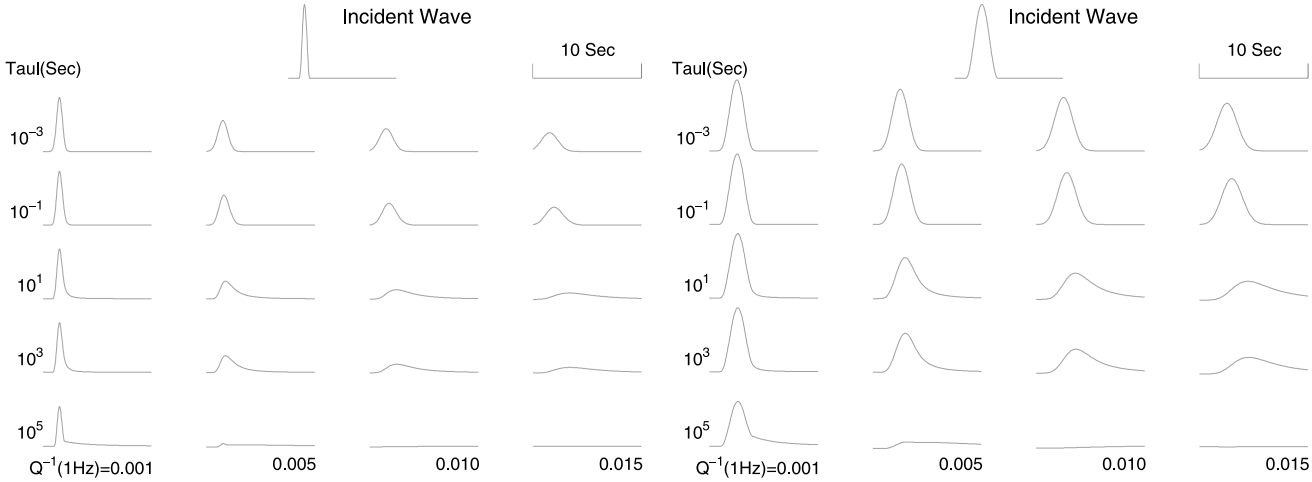


**Figure 4.** Attenuation operators convolved with a given wavelet. The travel distance is comparable to the diameter of the inner core. Amplitudes are normalized to the incident wavelet. (a) The incident wavelet has a 1 s duration. (b) The incident wavelet has a 3 s duration.

report experimental results for viscoelastic relaxations in bcc and fcc iron of the approximate magnitude of the seismically observed $Q^{-1}$ of the inner core. They suggest fcc and bcc iron as an alternative to the more widely favored hcp iron because of the higher intrinsic anisotropy of those phases, which makes it easier to satisfy the observed elastic anisotropy without invoking the existence of an inner-core sized crystal. Recent first principles calculations by *Steinle-Neumann et al.* [2001], however, find that it is not as difficult to reproduce the observed elastic anisotropy with hcp iron at inner core temperature. They also conclude that the high Poisson's ratio of the inner is consistent with the elastic constants of hcp iron at inner core conditions without invoking the effects of either viscoelastic dispersion or partial melt.

### 1.2. Limitations of Previous Seismic Studies

[7] Most previous studies are limited to just the uppermost few hundred kilometers of the inner core due to the difficulty of finding a good reference phase to study attenuation beyond 153°. Reference phases are those having rays that sample nearly the same path as PKIKP in the mantle but turn just above the inner core boundary. A reference phase can remove the effects of attenuation in the mantle, crustal structure near the source and receiver, and earthquake time history and fault orientation. The removal of these effects can be achieved by either forming the spectral ratio of the reference phase with PKIKP or by seeking the time domain operator needed to convert the reference phase into PKIKP. Common reference phases used in the study of inner core attenuation are PKP-BC and PKP-AB (Figure 1). In the distance range greater than 153°, PKP-BC will be diffracted, and PKP-AB will graze the D″ region of the lowermost mantle, a region of possible higher scattering or intrinsic attenuation. By being restricted to the narrow depth range of the inner core sampled by PKIKP at distances less than 153°, studies using PKP-BC as a reference phase often have difficulty in resolving the depth dependence of attenuation in measurements having a typically high variance [*Cormier*, 1981; *Niazi and Johnson*, 1992; *Bhattacharyya et al.*, 1993; *Souriau and Roudil*, 1995]. If PKP-AB is instead used as a reference phase to extend the depth region of study, it becomes difficult to resolve the ambiguity of the effects of attenuation in D″ from those of attenuation in the inner core.

[8] Furthermore, the reference phases following PKIKP are contaminated by the interference of depth phases (pP or sP) for shallow events whose paths are needed to obtain good global coverage of the inner core. Thus, most previous studies only process events having depths deep enough to insure that the depth phases pP and sP do not interfere with the reference phase. For a shallow earthquake with a depth of about 10 km, the time delays of pP and sP relative to first P arrivals are about several seconds, which is comparable to the travel time differences between PKP-DF and PKP-BC in the distance range of 145–153° (see Figure 1). With this criterion, more than 70 percent of earthquakes that occur in the shallow depth range of $0 \sim 70$ km will be eliminated, making it much more difficult to resolve any regional dependence or anisotropy of attenuation. Finally, in either the spectral ratio or time domain operator approach, scattered waves riding on top of the reference phases, will contribute to errors in estimated parameters and limit the bandwidth of study.

### 1.3. Approach of This Study

[9] A new approach is applied to investigate the attenuation in the deeper part of the inner core. Rather than using observed PKP-BC or PKP-AB phases as a reference phase, reference waveforms are synthesized for each observed PKIKP waveform from the source-time history and moment tensor inverted from network recorded P waveforms. These reference waveforms include the specific source-time history of the earthquake, local reverberations near the source and receiver, and the effect of a laterally homogeneous (network averaged) attenuation in the mantle. These synthetic reference waveforms are then used in an inversion for an attenuation operator in the inner core. By including

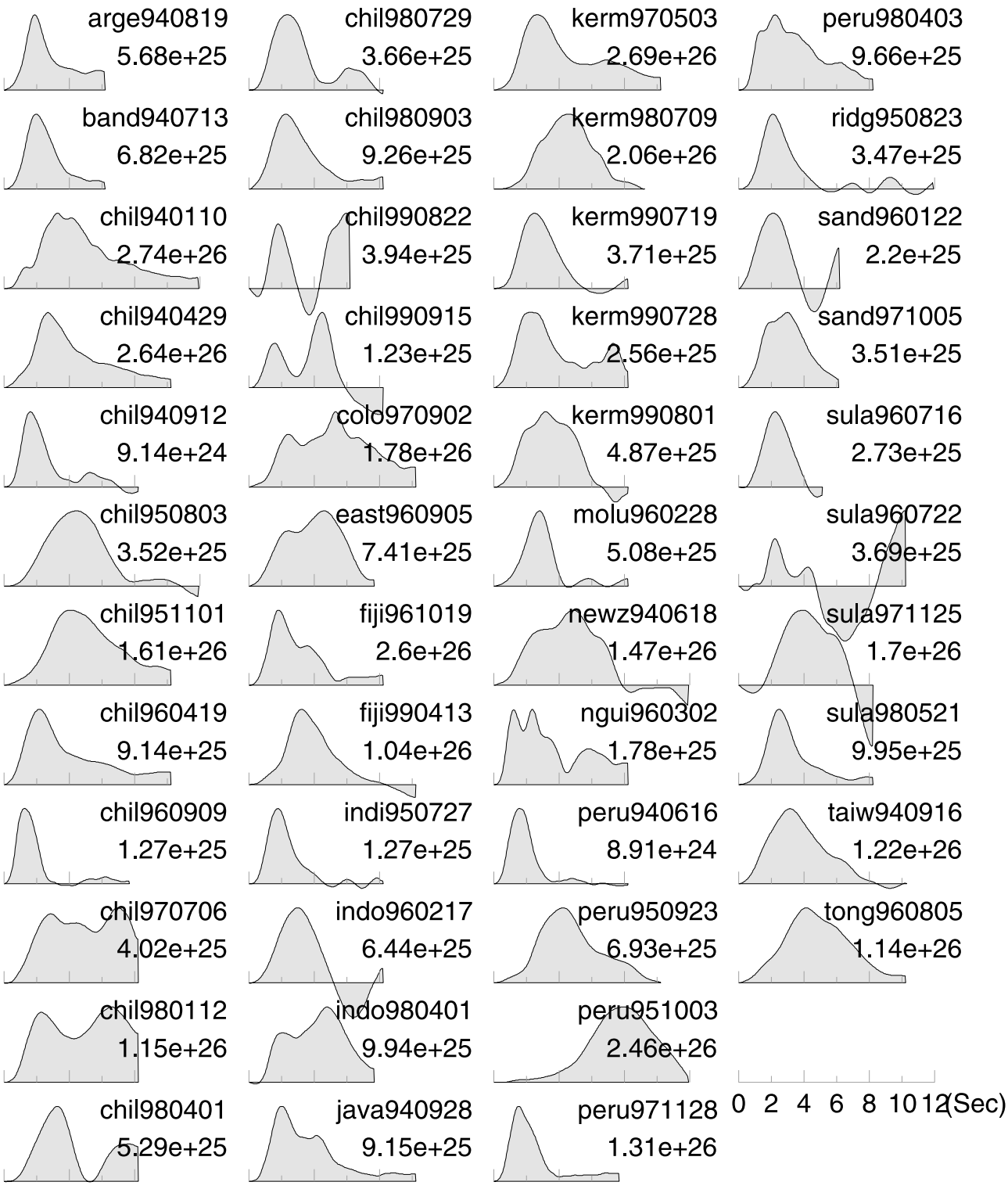


**Figure 5.** The inverted reference source time functions (RSTFs) for the 46 events used in this study. The event code (see Table 1) and the scalar moment in dyne-cm are given to the right of each displacement waveform. Inverted geometric source properties are given in Table 2.

waveform data up to antipodal range from both deep and shallow sources, this approach improves the resolution of the frequency dependence, depth dependence, and anisotropy of seismic attenuation in the inner core. Parameters are estimated for two possible physical mechanisms of seismic attenuation: intrinsic viscoelasticity (this paper) and scattering by a heterogeneous fabric in paper 2 [*Cormier and Li*, 2002]. In the scattering interpretation

**Table 1.** Earthquakes Processed for RSTFs

| Event Code | MM | DD | YY | hh | min | sec | Latitude, ° | Longitude, ° | Depth, km | $M_w$ |
|---|---|---|---|---|---|---|---|---|---|---|
| chil940110 | 1 | 10 | 94 | 15 | 53 | 49.6 | −13.31 | −69.39 | 589 | 6.9 |
| chil940429 | 4 | 29 | 94 | 7 | 11 | 30.3 | −28.3 | −63.17 | 573 | 6.9 |
| peru940616 | 6 | 16 | 94 | 18 | 41 | 31.3 | −15.18 | −70.34 | 225 | 5.9 |
| newz940618 | 6 | 18 | 94 | 3 | 25 | 19.5 | −42.86 | 171.46 | 9 | 6.7 |
| band940713 | 7 | 13 | 94 | 11 | 45 | 25.9 | −7.5 | 127.92 | 185 | 6.5 |
| arge940819 | 8 | 19 | 94 | 10 | 2 | 51.8 | −26.65 | −63.38 | 565 | 6.5 |
| chil940912 | 9 | 12 | 94 | 6 | 29 | 56.3 | −31.13 | −71.64 | 46 | 5.9 |
| taiw940916 | 9 | 16 | 94 | 6 | 20 | 18.3 | 22.55 | 118.74 | 12 | 6.7 |
| java940928 | 9 | 28 | 94 | 16 | 39 | 52.2 | −5.77 | 110.33 | 643 | 6.6 |
| indi950727 | 7 | 27 | 95 | 5 | 51 | 17.9 | −12.58 | 79.24 | 26.5 | 6 |
| chil950803 | 8 | 3 | 95 | 1 | 57 | 21.7 | −23.13 | −70.6 | 27 | 6.3 |
| ridg950823 | 8 | 23 | 95 | 13 | 14 | 45.6 | −56.75 | −141.68 | 15 | 6.3 |
| peru950923 | 9 | 23 | 95 | 22 | 31 | 58.3 | −10.53 | −78.7 | 73 | 6.5 |
| peru951003 | 10 | 3 | 95 | 1 | 51 | 24.1 | −2.77 | −77.88 | 27 | 7 |
| chil951101 | 11 | 1 | 95 | 0 | 35 | 32.3 | −28.96 | −71.5 | 20 | 6.7 |
| sand960122 | 1 | 22 | 96 | 23 | 20 | 1.2 | −60.62 | −25.73 | 21 | 6.2 |
| indo960217 | 2 | 17 | 96 | 14 | 21 | 23.7 | −0.59 | 135.87 | 15 | 6.5 |
| molu960228 | 2 | 28 | 96 | 9 | 44 | 9.4 | 1.73 | 126.1 | 103 | 6.4 |
| ngui960302 | 3 | 2 | 96 | 1 | 50 | 4.5 | −5.97 | 146.57 | 36 | 6.1 |
| chil960419 | 4 | 19 | 96 | 0 | 19 | 31.1 | −23.94 | −70.09 | 45 | 6.6 |
| sula960716 | 7 | 16 | 96 | 10 | 7 | 36.6 | 1.02 | 120.25 | 21 | 6.2 |
| sula960722 | 7 | 22 | 96 | 14 | 19 | 35.7 | 1 | 120.45 | 28.6 | 6.3 |
| tong960805 | 8 | 5 | 96 | 2 | 8 | 58.2 | −15.27 | −173.13 | 53 | 6.7 |
| east960905 | 9 | 5 | 96 | 8 | 14 | 14.4 | −22.12 | −113.44 | 14 | 6.5 |
| chil960909 | 9 | 9 | 96 | 0 | 20 | 39.1 | −31.9 | −71.56 | 39 | 6 |
| fiji961019 | 10 | 19 | 96 | 14 | 53 | 48.7 | −20.41 | −178.51 | 591 | 6.9 |
| kerm970503 | 5 | 3 | 97 | 16 | 46 | 2 | −31.79 | −179.38 | 108 | 6.9 |
| chil970706 | 7 | 6 | 97 | 9 | 54 | 0.8 | −30.06 | −71.87 | 19.4 | 6.3 |
| colo970902 | 9 | 2 | 97 | 12 | 13 | 22.9 | 3.85 | −75.75 | 198.7 | 6.8 |
| sand971005 | 10 | 5 | 97 | 18 | 4 | 30 | −59.74 | −29.2 | 273.9 | 6.3 |
| sula971125 | 11 | 25 | 97 | 12 | 14 | 33.6 | 1.24 | 122.54 | 13 | 6.7 |
| peru971128 | 11 | 28 | 97 | 22 | 53 | 41.5 | −13.74 | −68.79 | 586 | 6.7 |
| chil980112 | 1 | 12 | 98 | 10 | 14 | 7.6 | −30.99 | −71.41 | 35 | 6.6 |
| chil980401 | 4 | 1 | 98 | 22 | 42 | 56.9 | −40.32 | −74.87 | 9 | 6.4 |
| indo980401 | 4 | 1 | 98 | 17 | 56 | 23.4 | −0.54 | 99.26 | 46.7 | 6.6 |
| peru980403 | 4 | 3 | 98 | 22 | 1 | 48.2 | −8.15 | −74.24 | 150.6 | 6.6 |
| sula980521 | 5 | 21 | 98 | 5 | 34 | 25.5 | 0.21 | 119.59 | 26 | 6.6 |
| kerm980709 | 7 | 9 | 98 | 14 | 45 | 40 | −30.49 | −178.99 | 146 | 6.8 |
| chil980729 | 7 | 29 | 98 | 7 | 14 | 24.1 | −32.31 | −71.29 | 52.1 | 6.3 |
| chil980903 | 9 | 3 | 98 | 17 | 37 | 58.2 | −29.45 | −71.71 | 27 | 6.6 |
| fiji990413 | 4 | 13 | 99 | 10 | 38 | 47 | −21.38 | −176.54 | 163 | 6.6 |
| kerm990719 | 7 | 19 | 99 | 2 | 17 | 5 | −28.58 | −177.61 | 52 | 6.3 |
| kerm990728 | 7 | 28 | 99 | 10 | 8 | 21 | −30.24 | −177.98 | 40 | 6.2 |
| kerm990801 | 8 | 1 | 99 | 8 | 39 | 8 | −30.44 | −177.84 | 14 | 6.4 |
| chil990822 | 8 | 22 | 99 | 9 | 35 | 39 | −40.42 | −74.82 | 10 | 6.3 |
| chil990915 | 9 | 15 | 99 | 3 | 1 | 24 | −20.68 | −67.14 | 220 | 6 |

of paper 2, models of 1-D and 3-D fabric are constructed to infer velocity variations and scale lengths in the inner core.

## 2. Modeling

### 2.1. Absorption Band Model

[10] Intrinsic attenuation is the energy lost to heat and internal friction during the passage of elastic waves. Physical processes of intrinsic attenuation include thermoelasticity, diffusion of dislocations and point/line defects, stress-induced ordering, phase changes, and twinning–detwinning [*Liu et al.*, 1976]. For any one of these processes in a polycrystalline aggregate such as the Earth, many different characteristic relaxation times are possible, and their superposition gives a spectrum of relaxation times. *Liu et al.* [1976], assuming a distribution of relaxation times, constructed a relaxation spectrum with a nearly constant $Q$ over a frequency band $(2\pi\tau_1)^{-1}$ to $(2\pi\tau_2)^{-1}$ (Figure 2). Such an absorption band model can explain observations of Q independent of frequency over some finite band.

[11] The absorption band model has had remarkable success in explaining the seismic attenuation of the Earth. For example, *Minster* [1978a, 1978b] described the peak amplitude, apparent arrival time, peak time and risetime of the attenuation operator as functions of the parameters characterizing the absorption band model. From observations and microphysical theory, *Lundquist and Cormier* [1980] and *Anderson and Given* [1982] provided constraints on the absorption band model and proposed frequency-dependent and depth-dependent attenuation models for the Earth's mantle. Using the absorption band model, *Doornbos* [1983] successfully predicted differences in travel time between long- and short-period recordings of body waves turning in the lower mantle. From observations at the NORSAR array, Doornbos also noted that the dispersion of PKIKP waves in the inner core is anomalously weak and modeled the dispersion by an absorption band with a low-

**Table 2.** Fault-Plane Solution Parameters Before and After Inversion for the Far-Field Source Representations Determined for the 46 Events for Which RSTFs Were Calculated (Only One of Two Nodal Planes is Given)[a]

| | Initial Values | | | | After Inversion | | | |
|---|---|---|---|---|---|---|---|---|
| Event Code | Strike, ° | Dip, ° | Rake, ° | Depth, km | Strike, ° | Dip, ° | Rake, ° | Depth, km |
| chil940110 | 99.0 | 77.0 | −83.0 | 589.0 | 77.8 | 75.4 | −66.2 | 589.0 |
| chil940429 | 170.0 | 72.0 | −100.0 | 573.0 | 134.3 | 86.3 | −60.4 | 573.0 |
| peru940616 | 50.0 | 81.0 | 152.0 | 225.0 | 3.8 | 69.5 | 174.7 | 225.0 |
| newz940618 | 68.0 | 63.0 | 150.0 | 9.0 | 70.4 | 88.7 | 163.4 | 5.5 |
| band940713 | 312.0 | 42.0 | 131.0 | 185.0 | 333.3 | 54 | 145.7 | 185.0 |
| arge940819 | 159.0 | 73.0 | −107.0 | 565.0 | 159.7 | 70.3 | −83.9 | 565.0 |
| chil940912 | 167.0 | 74.0 | 103.0 | 46.0 | 163.2 | 73.5 | 72.4 | 46.7 |
| taiw940916 | 256.0 | 35.0 | −116.0 | 12.0 | 274.6 | 34.5 | −95.1 | 13.3 |
| java940928 | 68.0 | 54.0 | −143.0 | 643.0 | 68.3 | 54.9 | −141.9 | 643.0 |
| indi950727 | 275.0 | 33.0 | 135.0 | 26.5 | 287.8 | 35.5 | 121.1 | 26.3 |
| chil950803 | 168.0 | 79.0 | 85.0 | 27.0 | 186.1 | 70.7 | 44.7 | 23.6 |
| ridg950823 | 258.0 | 63.0 | −62.0 | 15.0 | 221.5 | 53 | −102.1 | 17.1 |
| peru950923 | 358.0 | 70.0 | −93.0 | 73.0 | 356.7 | 72.1 | −59.4 | 72.3 |
| peru951003 | 18.0 | 57.0 | 68.0 | 27.0 | 188.4 | 33.8 | 107.6 | 19.8 |
| sand960122 | 218.0 | 62.0 | −154.0 | 21.0 | 218.8 | 62.4 | −155 | 21.6 |
| indo960217 | 304.0 | 77.0 | 93.0 | 15.0 | 309.7 | 77.6 | 74.1 | 16.0 |
| molu960228 | 251.0 | 53.0 | 85.0 | 103.0 | 278.6 | 63.4 | 110.8 | 103.0 |
| ngui960302 | 289.0 | 47.0 | 86.0 | 36.0 | 340.5 | 55.2 | 126.1 | 36.9 |
| chil960419 | 171.0 | 62.0 | 83.0 | 45.0 | 163.4 | 69.8 | 86.4 | 48.6 |
| sula960716 | 264.0 | 77.0 | 96.0 | 21.0 | 262.2 | 74.9 | 90.2 | 20.3 |
| sula960722 | 264.0 | 77.0 | 96.0 | 28.6 | 231.6 | 83.6 | 29.3 | 27.3 |
| tong960805 | 124.0 | 64.0 | −69.0 | 53.0 | 182.9 | 60.5 | −114.5 | 50.0 |
| east960905 | 303.0 | 49.0 | 110.0 | 14.0 | 348 | 27.3 | 121.8 | 11.2 |
| chil960909 | 334.0 | 40.0 | 55.0 | 39.0 | 337.9 | 45.3 | 56.4 | 40.4 |
| fiji961019 | 13.0 | 67.0 | −77.0 | 591.0 | 18.4 | 70.3 | −48 | 591.0 |
| kerm970503 | 125.0 | 46.0 | −147.0 | 108.0 | 105.6 | 55.5 | −121.3 | 104.7 |
| chil970706 | 178.0 | 69.0 | 89.0 | 19.4 | 165.9 | 66.1 | 76.5 | 19.3 |
| colo970902 | 115.0 | 49.0 | 117.0 | 198.7 | 171.6 | 54.4 | 105 | 198.7 |
| sand971005 | 152.0 | 57.0 | −102.0 | 273.9 | 142.2 | 62.2 | −93.7 | 273.9 |
| sula971125 | 275.0 | 69.0 | 89.0 | 13.0 | 254.4 | 72.2 | 63.9 | 14.1 |
| peru971128 | 118.0 | 88.0 | −81.0 | 586.0 | 120.9 | 89.9 | −94.3 | 586.0 |
| chil980112 | 174.0 | 63.0 | 90.0 | 35.0 | 148.1 | 53.1 | 98.9 | 33.6 |
| chil980401 | 199.0 | 44.0 | −88.0 | 9.0 | 185.7 | 34.9 | −104.3 | 9.9 |
| indo980401 | 124.0 | 69.0 | 84.0 | 46.7 | 119.6 | 69.8 | 82.7 | 46.7 |
| peru980403 | 172.0 | 87.0 | 77.0 | 150.6 | 168.6 | 82.4 | 105.7 | 150.6 |
| sula980521 | 108.0 | 64.0 | 160.0 | 26.0 | 100.4 | 67.7 | 160.7 | 24.5 |
| kerm980709 | 15.0 | 75.0 | −97.0 | 146.0 | 19.3 | 81.2 | −87.7 | 146.0 |
| chil980729 | 309.0 | 55.0 | 74.0 | 52.1 | 323.7 | 58.5 | 85.6 | 56.8 |
| chil980903 | 199.0 | 76.0 | 105.0 | 27.0 | 199.1 | 68.2 | 60.3 | 31.0 |
| fiji990413 | 16.0 | 86.0 | −104.0 | 163.0 | 18.7 | 89.3 | −52.7 | 163.0 |
| kerm990719 | 28.0 | 61.0 | 92.0 | 52.0 | 43.9 | 52.7 | 95.7 | 61.9 |
| kerm990728 | 14.0 | 62.0 | 85.0 | 40.0 | 33.2 | 54.7 | 80.1 | 47.1 |
| kerm990801 | 16.0 | 69.0 | 84.0 | 14.0 | 64 | 79.5 | 100.5 | 14.0 |
| chil990822 | 14.0 | 46.0 | −96.0 | 10.0 | 27.3 | 44.6 | −110.5 | 10.8 |
| chil990915 | 351.0 | 82.0 | −70.0 | 220.0 | 355.8 | 86.8 | −54 | 220.0 |

[a] The initial values are taken from Harvard's CMT catalog.

frequency corner $(2\pi\tau_1)^{-1}$ of 2 Hz and a minimum $Q_\alpha$ of 100.

### 2.2. Parameterization

[12] In this study we adopt the absorption band model given by *Cormier and Richards* [1988]. The complex velocity $\hat{\alpha}(\omega)$ in this model is calculated by

$$\hat{\alpha}(\omega) = \alpha_0 \frac{\left[1 + \frac{2}{\pi} Q_m^{-1} D(\omega)\right]^{1/2}}{\left[1 + \frac{2}{\pi} Q_m^{-1} D(2\pi)\right]^{1/2}} \quad (1)$$

where

$$D(\omega) = \ln\left[\left(i\omega + \frac{1}{\tau_1}\right) \Big/ \left(i\omega + \frac{1}{\tau_2}\right)\right]$$

Here $\alpha_0$ is the reference velocity (at 1 Hz), a real number. $Q_m^{-1}$ is the peak attenuation and $\tau_1$, $\tau_2$ are cut-off relaxation times (correspondingly, $f_1 = 1/2\pi\tau_1$ and $f_2 = 1/2\pi\tau_2$ are the low and high frequency corners, respectively). The inverse $Q$ is obtained by

$$Q^{-1}(\omega) = 2\,\mathrm{Im}[\hat{\alpha}(\omega)]/\mathrm{Re}[\hat{\alpha}(\omega)] \quad (2)$$

[13] In the example shown in Figure 2, $\tau_1 = 0.1$ s, $\tau_2 = 10{,}000$ s and $Q_m^{-1} = 0.005$. Note that the strongest velocity dispersion correlates with constant attenuation and frequency-dependent attenuation correlates with near zero velocity dispersion. From equations (1) and (2) and Figure 2, we can see that this absorption model is fully controlled by three parameters, $\tau_1$, $\tau_2$ and $Q_m^{-1}$. Teleseismic

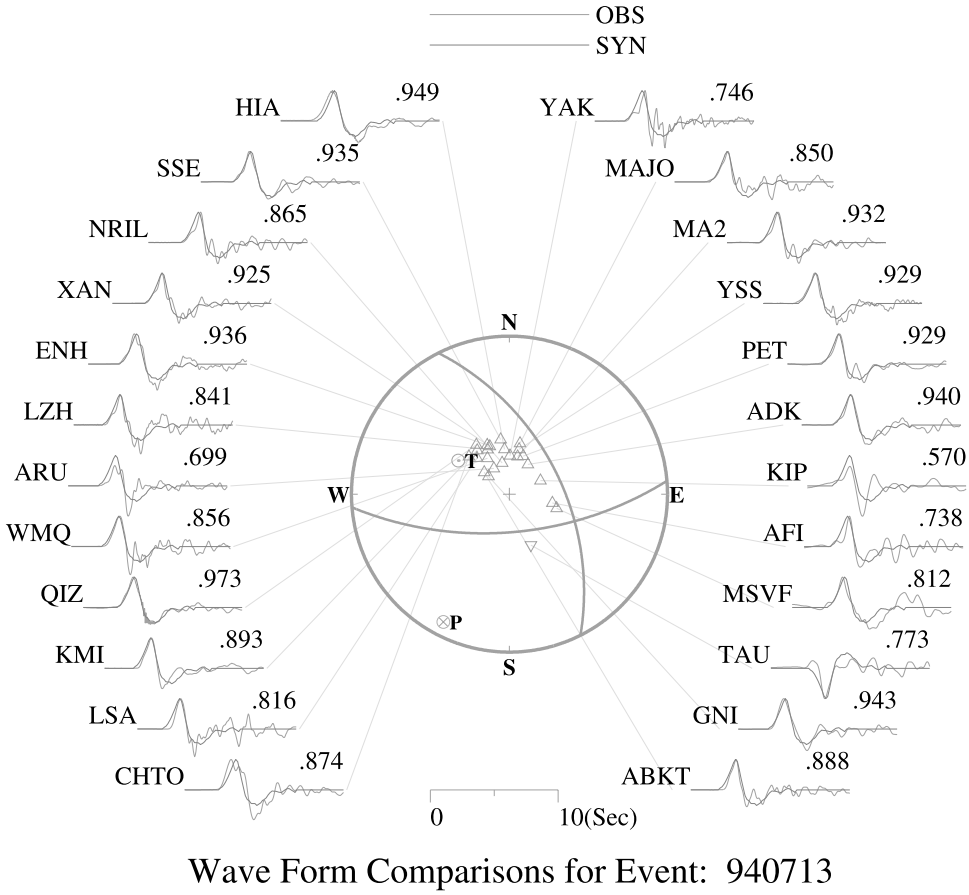


**Figure 6.** An example inversion for an RSFT. Waveform comparison, reference source time function, and source geometric properties of a 13 July 1994 Banda Sea earthquake.

body wave data, however, are generally very band-limited (0.02 to 2 Hz.), making the width of the absorption band given by the ratio ($\tau_1/\tau_2$) difficult to resolve. For models of the absorption band having widths that exceed the passband of data, predicted spectra can be almost identical in the frequency band of teleseismic body waves for quite different values of $\tau_1/\tau_2$. Since the data have little or no sensitivity to this ratio, we simply fix $\tau_1/\tau_2$ to $10^5$, following suggestions of *Anderson and Given* [1982]. We emphasize, however, that while the data cannot resolve the width of the relaxation spectrum, the frequency dispersion of velocity recovered from waveforms can determine whether either corner of the absorption band lies within the frequency band of data. Data lying near a corner of the absorption band are much less dispersed than data lying in the middle of the absorption band where attenuation is nearly constant with frequency.

[14] $Q^{-1}$ at 1 Hz is used as the other free parameter rather than the peak $Q_m^{-1}$. The relation between the peak attenuation and, $Q^{-1}$ at 1 Hz is controlled by equation (1) and is given by

$$Q_m^{-1} = \frac{2\pi q_1 \mathrm{Im}(D(\omega))}{(q_1^2 - 4)[\mathrm{Im}(D(\omega))]^2 + 4q_1 \mathrm{Im}(D(\omega))\mathrm{Re}(D(\omega))} \quad (3)$$

where $q_1 = Q^{-1}(1\ \mathrm{Hz})$. Thus the free two parameters we will consider are $\tau_1$ and $Q^{-1}$ at 1 Hz. (The ratio $\tau_1/\tau_2$ is fixed at $10^5$.) Figures 3a and 3b show how the velocity dispersion and attenuation vary in the teleseismic body wave band as functions of these two parameters. Increasing the $Q^{-1}$ at 1 Hz increases the amount of velocity dispersion and attenuation. With increasing $\tau_1$, the relaxation spectrum will be shifted from low to high frequency. Figures 4a and 4b show how waveforms appear when the attenuation operators corresponding to the parameters listed in Figures 3a and 3b are convolved with two different wavelets. The travel time is comparable to that of antipodal PKIKP waves in the inner core. With increasing $\tau_1$ and $Q^{-1}$ at 1 Hz, the amplitude generally decreases and the pulse duration increases.

## 3. Inversion

### 3.1. Reference Source Time Function

[15] In an earlier study [*Cormier et al.*, 1998] we used empirical reference source-time functions (RSTFs) obtained from P waveforms to invert for inner core attenuation. Ideally, the empirical source-time functions should be observed at ranges close to core-grazing and at nearly the same azimuth as that of the PKIKP waves to be inverted for attenuation parameters. Unfortunately the distribution of sources and receivers rarely makes this possible, and

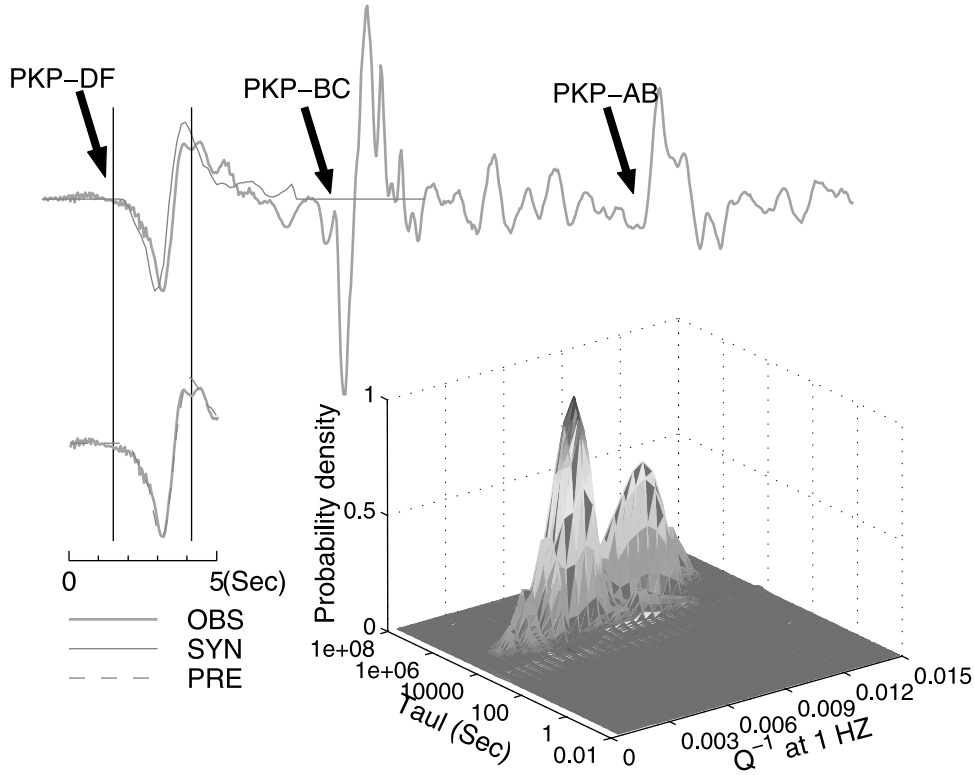


**Figure 7.** Inversion for the attenuation model parameters $Q^{-1}$(1 Hz) and $\tau_1$ maximizes a Gaussian probability density based on a least square norm [*Tarantola*, 1987]. The time window for inversion (thick vertical lines) is manually determined, generally consisting of the first-half cycle of a broadband velocity waveform.

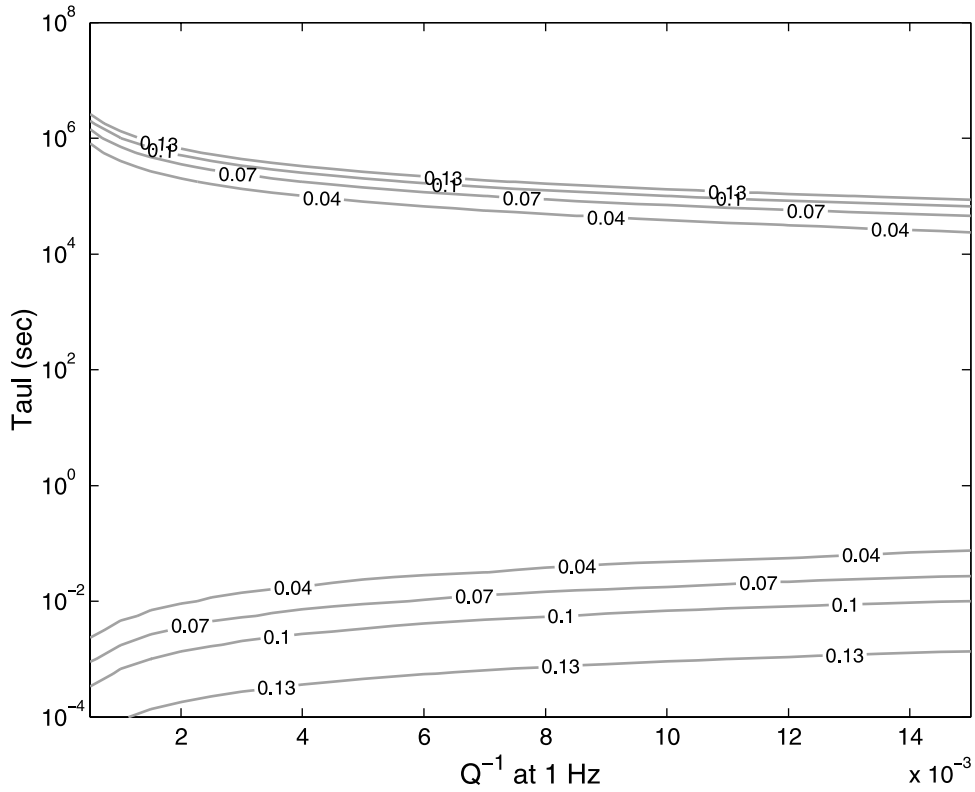


**Figure 8.** Contours of the maximum $Q^{-1}$ attenuation for an absorption band model as a function of $Q^{-1}$(1 Hz) and the low frequency corner $\tau_1$. To satisfy the constraint that $Q^{-1} < 0.07$, a reasonable range of $\tau_1$ is $10^{-3}$ to $10^{6}$ s.

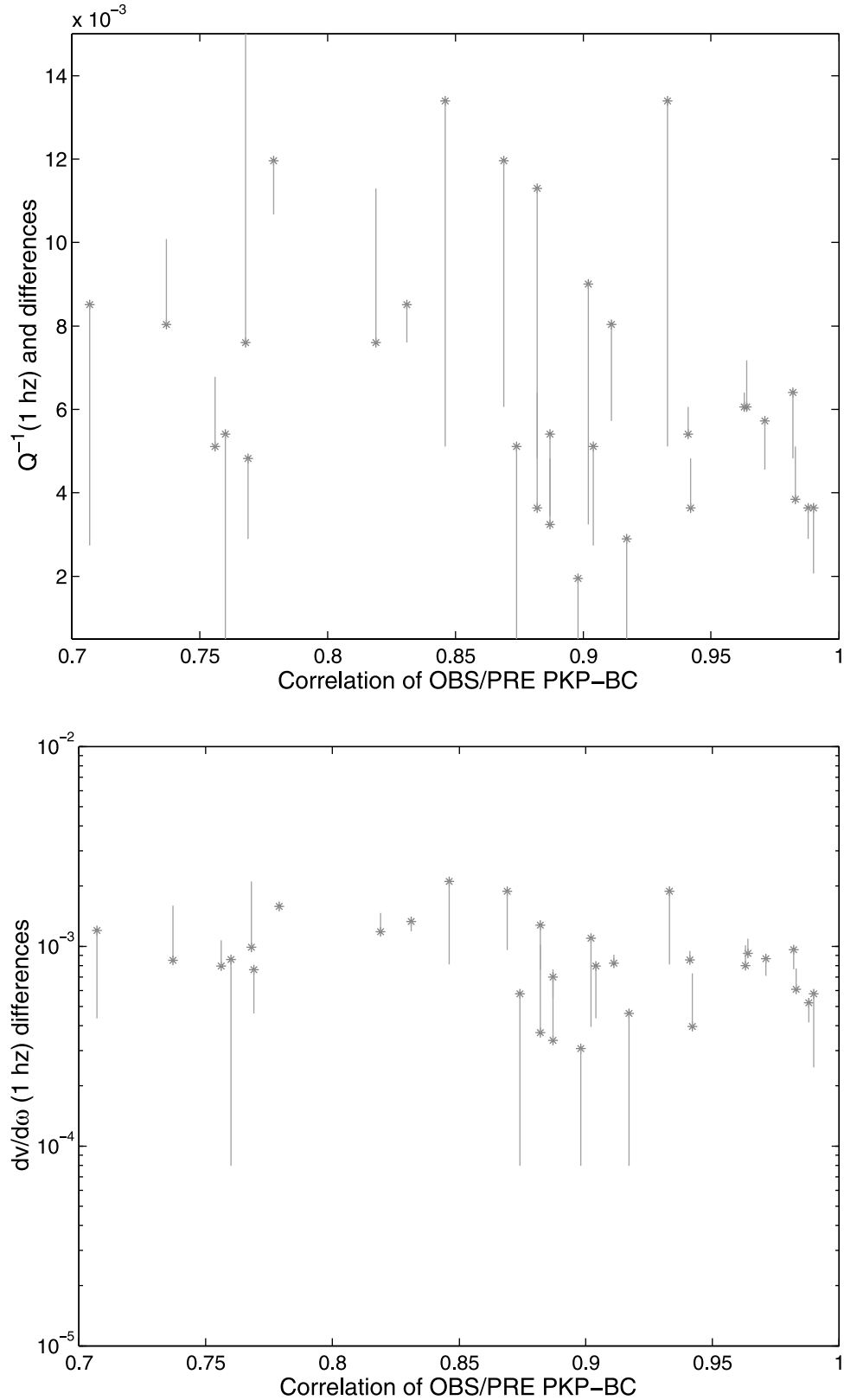


**Figure 9.** (a) Plots of $Q^{-1}$ and the dispersion parameter $d\alpha/d\omega$ (b) inverted from PKP-DF using reference source time functions (plotted symbols) and PKP-BC (end-point of lines emanating from plotted symbols) versus the cross-correlation of observed PKP-BC with the predicted PKP-BC (RSTF) at stations surrounding the 150° range.

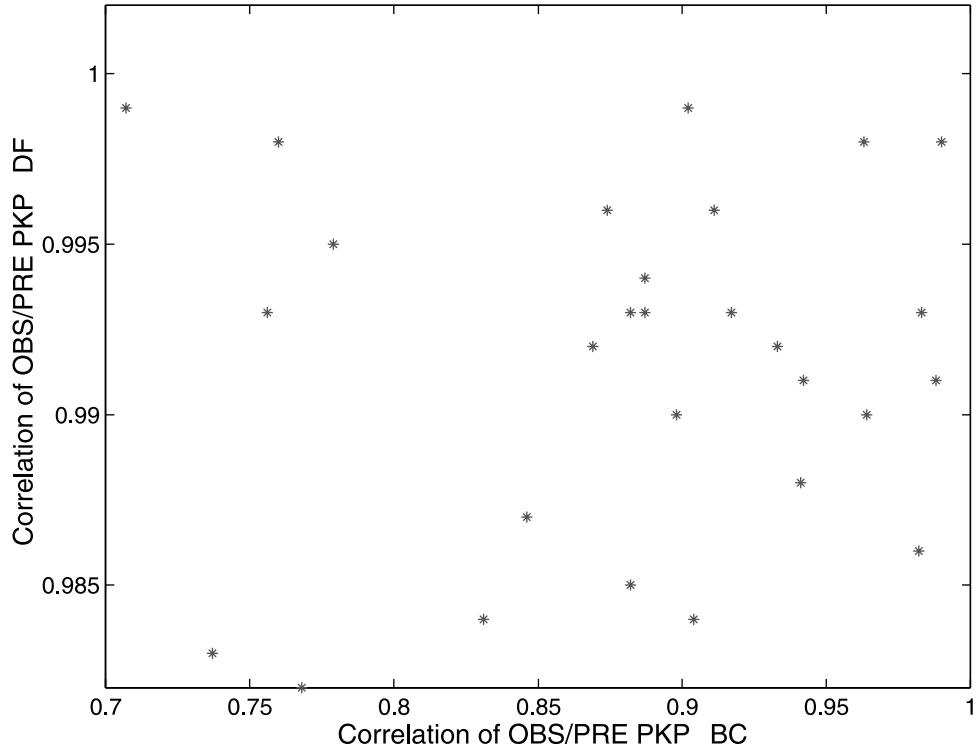


**Figure 10.** Cross-correlation of observed with predicted PKP-DF using RSTFs versus the cross-correlation of observed with predicrted PKP-DF using PKP-BC as the reference waveform.

departure from these ideal conditions will make the ray-directional variations in the source radiation and excitation of near source and receiver multiples contribute to errors in the estimated attenuation parameters.

[16] In the current study we predict the RSTFs for each station recording a PKIKP by first inverting the P waves observed in the range for 35°–85° for the best fitting teleseismic point source representation of the source-time function [*Langston and Helmberger*, 1975; *Barker and Langston*, 1982, 1983]. Starting solutions in the iterative inversions assumed the centroid moment tensors reported either by Harvard or the USGS. Figure 5 shows the results

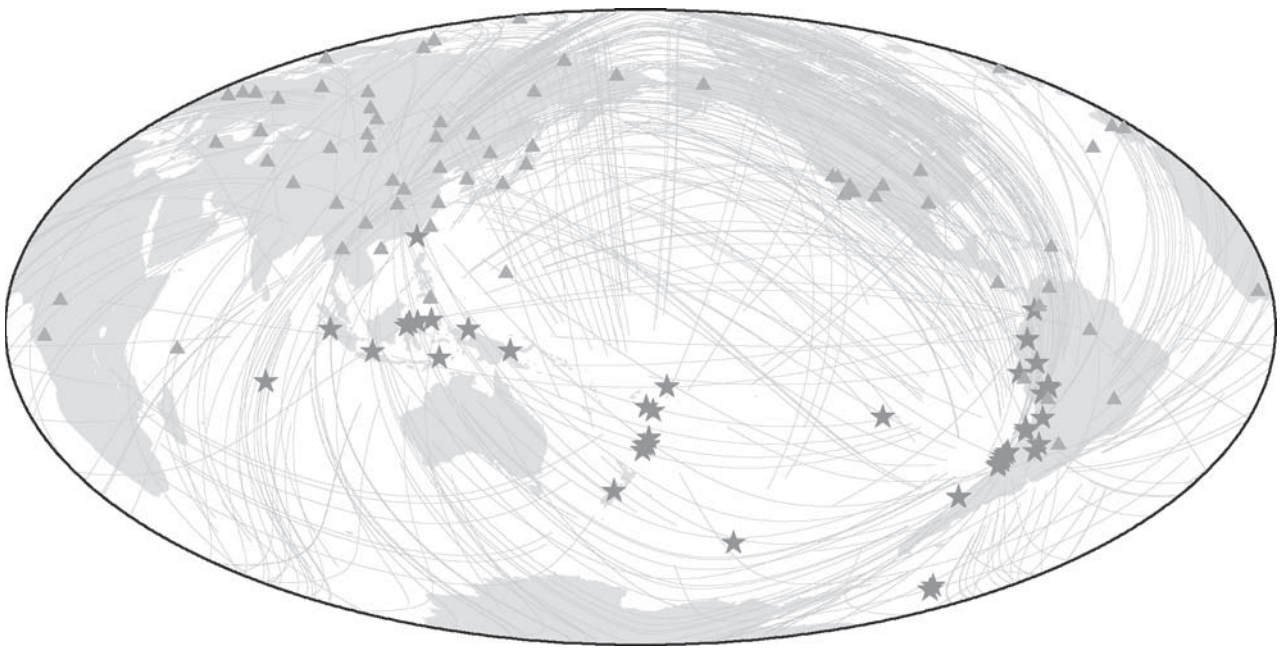

**Figure 11.** 345 PKIKP ray paths in the inner core used in the inversion for a viscoelastic attenuation model.

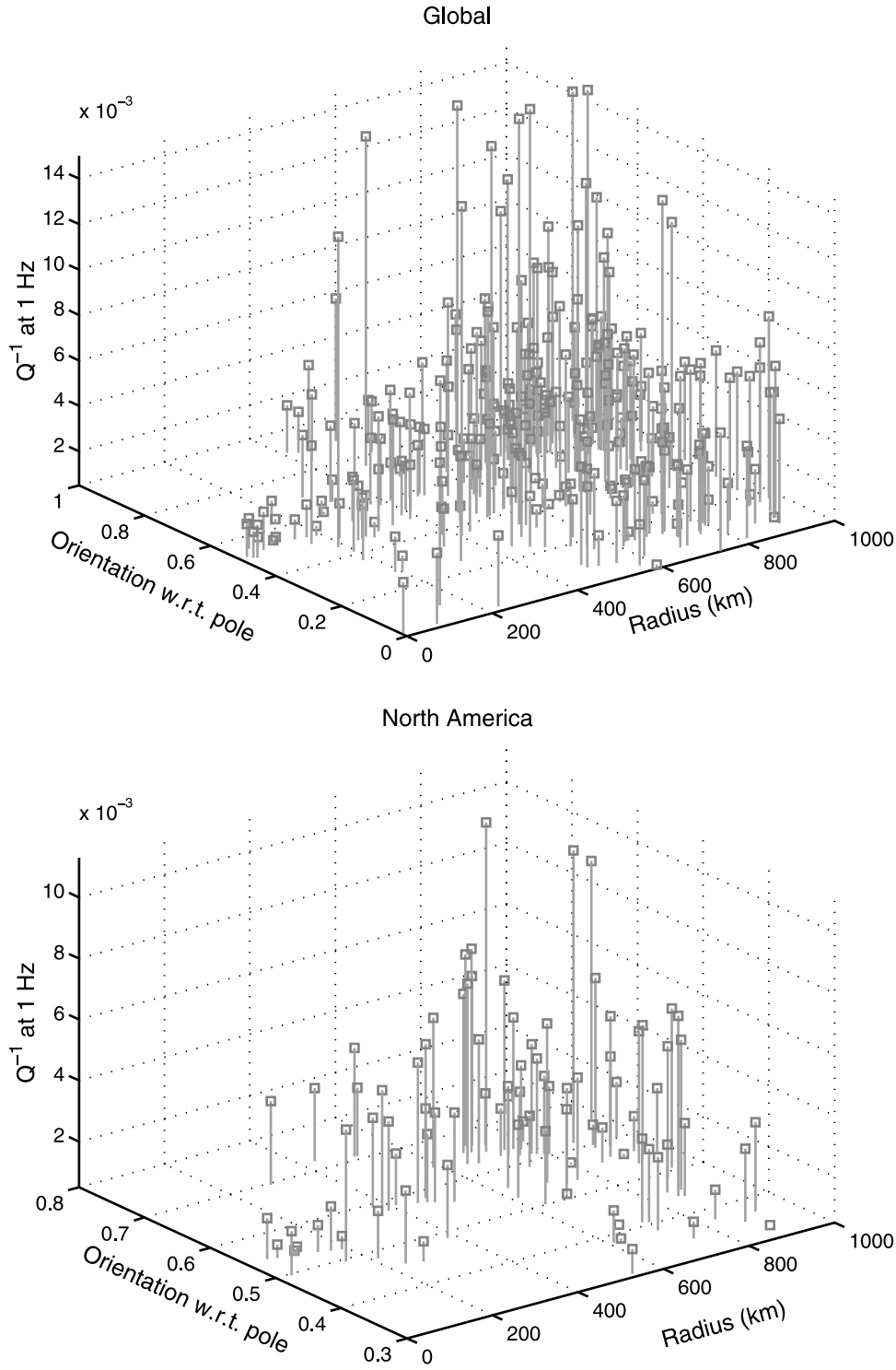


**Figure 12.** The variation of $Q^{-1}$(1 Hz) as a function of radius and ray direction at the turning point of the PKIKP ray path for (a) global, (b) North American, and (c) eastern Asia data, respectively. The ray direction is quantified by the dot product of the ray tangent at the turning point with the direction of the Earth's rotation axis.

obtained for the source-time functions for the 46 events (Tables 1 and 2) used in the study. Figure 6 shows an example fit to observed P waves from one of the events used in the study. Note that the negative excursions seen in the later portions of the displacement pulses shown in Figure 6 are the likely the result of unmodeled near-source or near-receiver scattering. These portions of the RSTFs are not used in the later inversion for inner core attenuation.

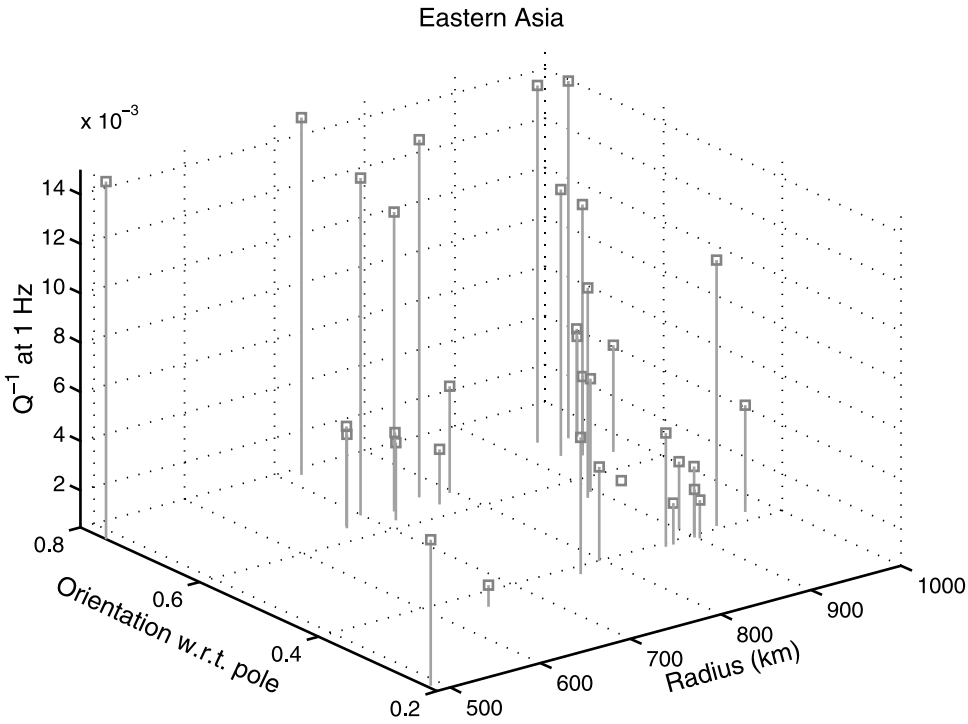


**Figure 12.** (continued)

Only the first half-cycle of PKIKP velocity pulses is used in the attenuation inversion.

### 3.2. Inversion for the Attenuation Operator

[17] After inversion for the teleseismic point-source representation, RSTFs, which include a network averaged mantle attenuation are constructed for the stations having PKIKP waveforms. An observed PKIKP wave is assumed to be of the form

$$U(t) = \mathrm{RSTF}(t) * A_I(t)$$

The function RSTF($t$) includes the source-time function, free surface reflections and reverberations near the source, and a network averaged mantle attenuation operator. Near source reverberations are calculated in crustal models that are customized for each source, including appropriate water layer thickness for oceanic sources. An average continental crust is assumed beneath each receiver. The RSTFs are inverted from P waves that turn below the upper mantle phase transitions ($\Delta > 35°$) and above an assumed 150 km thick D″ ($\Delta < 85°$). $A_I(t)$ is the attenuation operator given by the inverse Fourier transform of the operator $A_I(\omega) = \exp[i\omega\int(1/\alpha(\omega))ds]$, where $\alpha(\omega)$ is the complex velocity given by equation (1) and the path integral is taken over the inner core portion of the PKIKP ray path.

[18] The inversion for $A_I(t)$ searches for model parameters that maximize a Gaussian probability density based on the least squares norm [*Tarantola*, 1987]. The errors are measured by the 95% confidence limits. In the time window, the amplitudes of observed and synthetic signals are normalized, so that the search for optimal attenuation parameters results in a best waveform fit. Only the signal in the first half cycle of the velocity waveform is fit to eliminate the possible interference by unmodeled scattering near the source and receiver. Figure 7 illustrates the inversion procedure for intrinsic attenuation, in which two attenuation parameters are sought. The inversion for scattering attenuation described in Paper 2 is similar except for a search for different types of model parameters.

[19] Even though the best waveform fits are found in this method, the fitting process by itself ignores the amplitude ratio of the observed to synthetic signals, which is also available to give an important constraint. No matter how much uncertainty may exist in the data and model, it is unrealistic to expect a factor of ten or more in this amplitude ratio. Thus, in the inversion procedure we set the criterion of acceptability for this ratio to 10 for the ratio of observed to synthetic seismogram.

### 3.3. Searching Ranges and Intervals

[20] It is inefficient to map the probability density of parameters whose bounds are too large and or intervals are too small. Thus, reasonable searching ranges and intervals should be specified so that the maximum probability density will fall around the center of the searching range and the best fit will be obtained in a reasonable computation time. Establishment of reasonable search ranges is also essentially equivalent to *Tarantola*'s [1987] specification of a priori model covariance.

[21] The bounds on intrinsic attenuation can be set from the range of observed $Q^{-1}$ reported for the inner core. These range in the interval of $0.002 \sim 0.01$ for PKIKP waves. Allowing for extreme values at either end of this range, the searching range for $Q^{-1}$ at 1 Hz is set as 0.0005 to 0.015. Bounds on the searching range of $\tau_1$ are established from the assumed fixed value of $\tau_1/\tau_2$ and the theory of viscoelasticity. Viscoelasticity imposes an upper bound on the constant $Q^{-1}$ in the flat portion of the relaxation spectrum. This bound on $Q^{-1}$ is given by physical limits on the difference between the unrelaxed and relaxed velocities. The existence

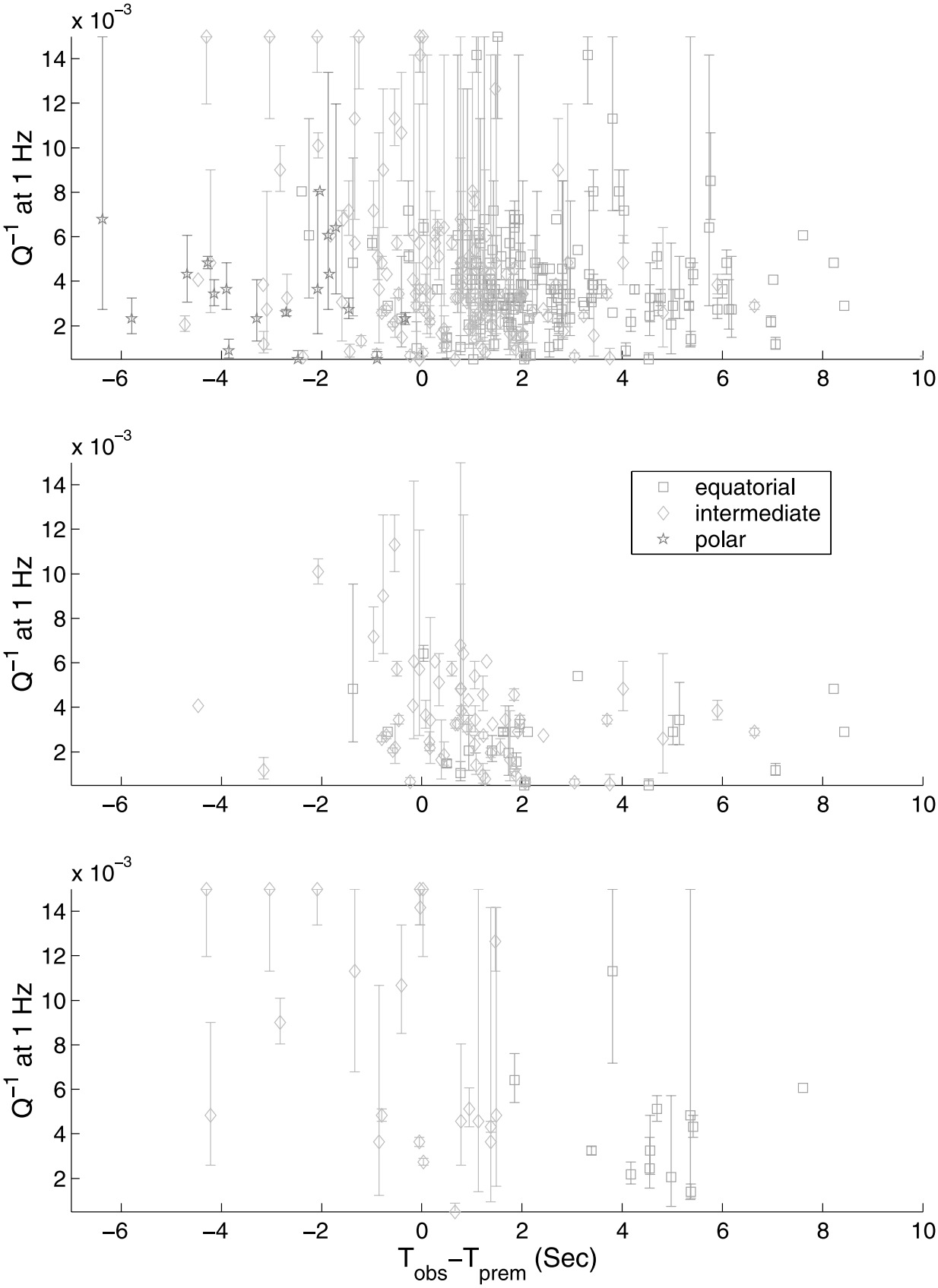


**Figure 13.** Attenuation and travel time residual Tobs − Tpred, where Tpred is from PREM [*Dziewonski and Anderson*, 1981]. (a) Upper: Global data; (b) Middle: North American data; (c) lower: eastern Asia data. Symbols in the legend group results by ray direction of PKIKP turning points with respect to the rotational axis.

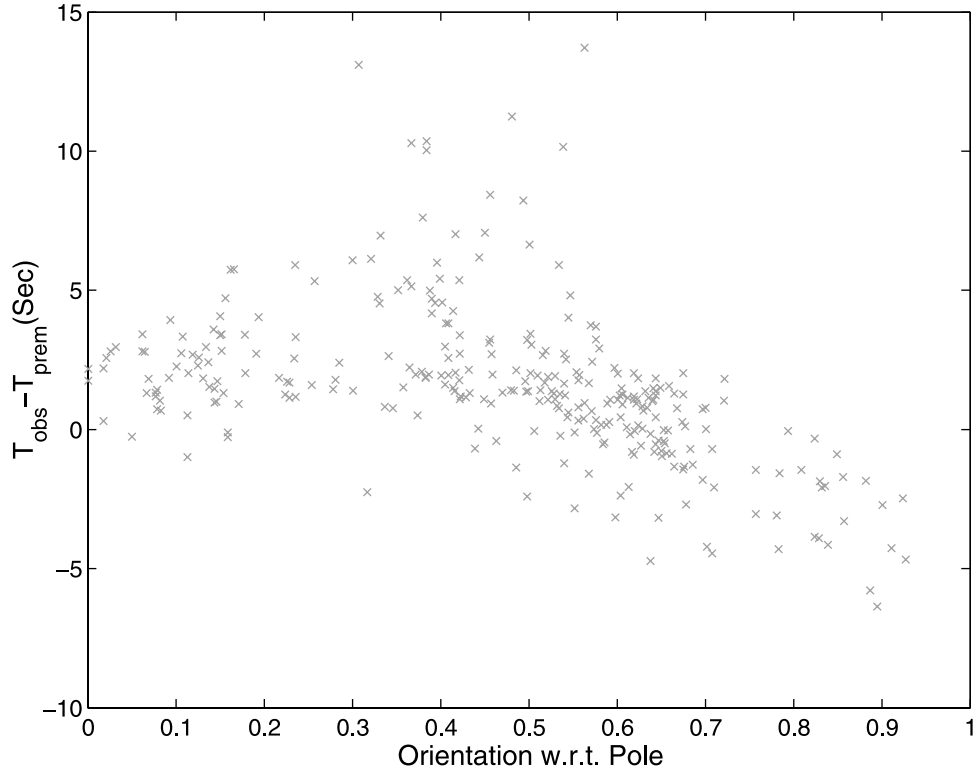


**Figure 14.** PKIKP travel time residual Tobs − Tpred versus ray direction at the turning point (1 is polar; 0 equatorial).

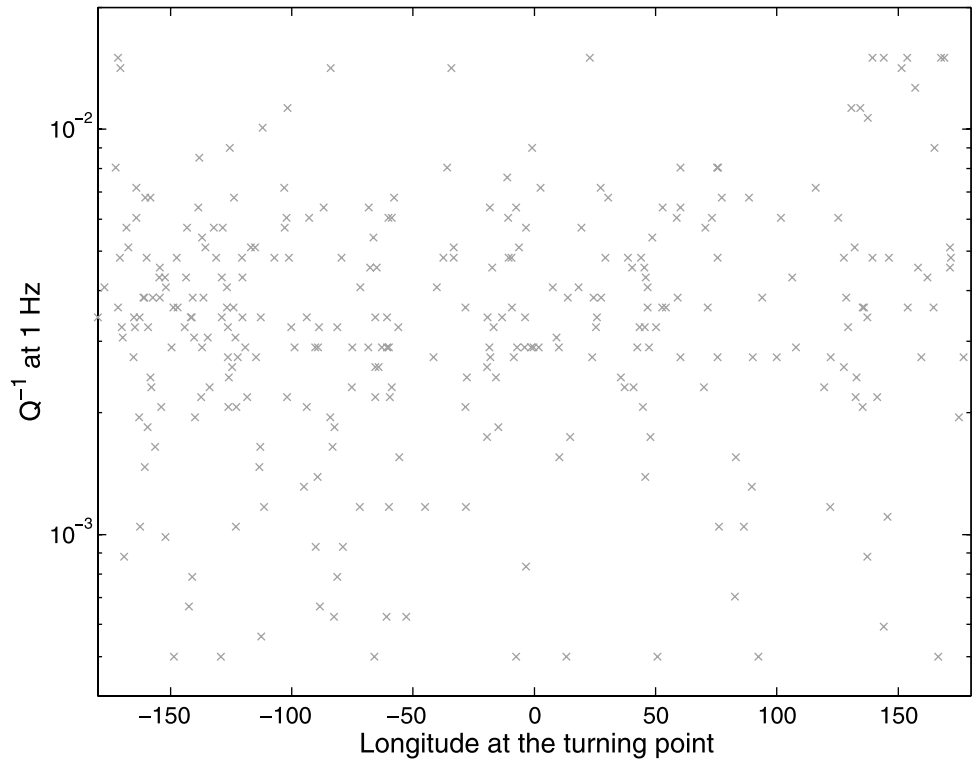


**Figure 15.** The attenuation in the inner core versus longitude at the turning point of the PKIKP ray path.

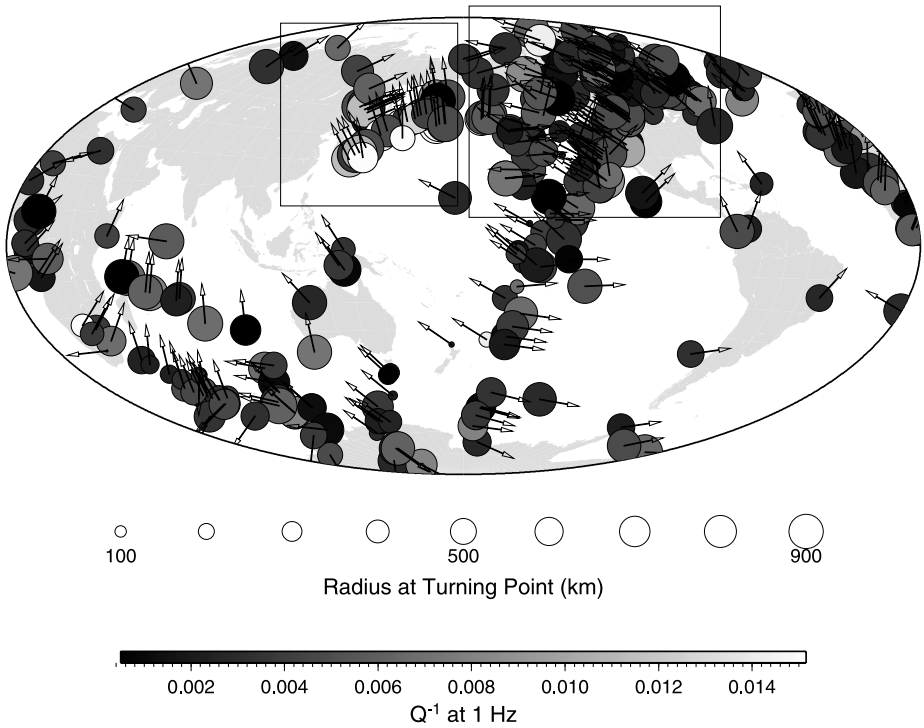


**Figure 16.** Global distribution of inverted $Q^{-1}$(1 Hz) plotted at the ray turning points. The arrow on each result indicates the ray direction at the turning point. The two dashed rectangles indicate the areas where regional analyses are compared: North America (right) and eastern Asia (left).

of a relaxation implies a particular "modulus defect" given by the difference in the elastic modulus at the low frequency limit (relaxed modulus) and high frequency limit (unrelaxed modulus). From viscoelastic theory, the maximum constant $Q^{-1}$ should satisfy [*Minster*, 1980; *Chin*, 1980]

$$Q_{\max}^{-1} = \Delta \frac{\pi}{2 \ln\left(\frac{\tau_1}{\tau_2}\right)} \tag{4}$$

where $\Delta$ is the fractional modulus defect. Its value is generally around $20 \sim 25\%$, and may be increased for some cases [*O'Connell*, 1978]. If $\Delta = 50\%$ is an extreme case, the maximum constant $Q^{-1}$ should be less than 0.07 for the assumed fixed value of $\tau_1/\tau_2 = 10^5$. With this constraint, a reasonable searching range for $\tau_1$ is determined to be $10^{-3} \sim 10^6$ s (Figure 8).

[22] Because of the large range of the parameters, the searching grids for both parameters are arranged as a geometric series:

$$x_i = x_{\min} q^{i-1} \text{ where } q = e^{\ln(x_{\max}/x_{\min})/(N-1)} \tag{5}$$

Here, $x$ indicates either $\tau_1$ or $Q^{-1}$ at 1 Hz. $N$ is the number of discrete numbers. After testing, we set $N = 41$ for $\tau_1$ and $N = 61$ for $Q^{-1}$ at 1 Hz for the results to have an acceptable resolution and affordable computation time.

### 3.4. Postprocessing and Review

[23] After inversion, we review the parameters for both the intrinsic model and the scattering model to determine if they lie in physically reasonable bounds. Five criteria were used in this review: (1) results that fall exactly at the boundaries of the parameter search domain are excluded because the true values may be beyond the bounds; (2) results with large estimated errors are eliminated; (3) correlation coefficients of observed and synthetic seismograms are required to be larger than 90%; (4) maximum signal-to-noise ratio in the frequency domain is required to be larger than a threshold value of 2; (5) rays with epicentral distance less than 150° are eliminated. (When $\Delta < 150°$, the amplitudes of PKIKP are generally too small relative to those of the PKP-BC branches, and the time delay between these two phases is very small.) Given these criteria, the postprocessing gives a total of 345 and 262 available results out of 393 PKIKP rays for the viscoelastic model and scattering model, respectively.

### 3.5. Comparison of Results Using RSTFs Versus PKP-BC

[24] Attenuation parameters inverted using predicted source-time functions and an average mantle attenuation operator were compared with the attenuation parameters inverted using the more common procedure of using PKP-BC waveforms as the reference source-time function. Figure 9 plots differences in the inverted attenuation parameters obtained using the two different types of reference waveforms against the correlation between the observed PKP-BC and the predicted PKP-BC waveform (RSTF). Not surprisingly, when the correlation between observed and predicted PKP-BC waveform is 95% or higher, the differences between the inverted attenuation parameters obtained by the two different methods are small. Since results for inverted parameters from waveform correlations less than 90% (this study) or 95% [*Bhattacharyya et al.*, 1993] are commonly discarded, we conclude that our RSTFs do not introduce any serious bias compared to results obtained from the use of PKP-BC as a reference waveform. Figure 10 shows that the

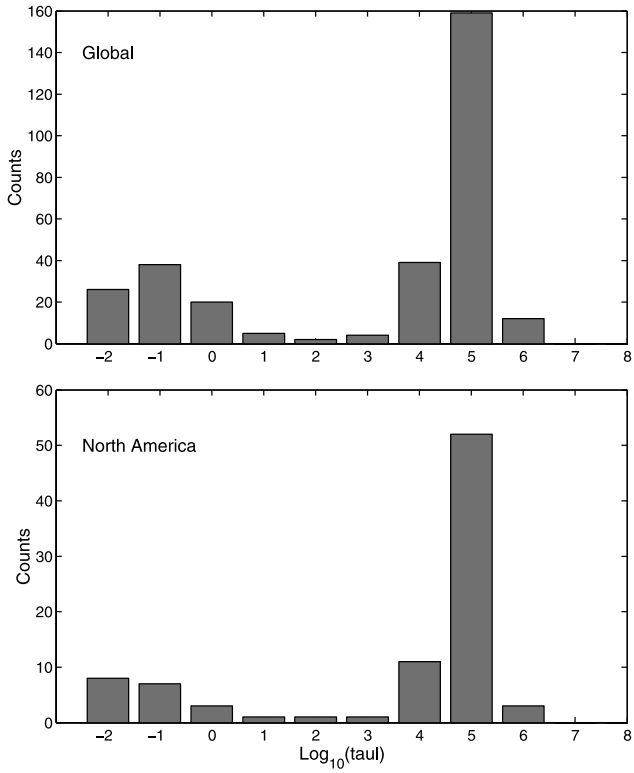


**Figure 17.** The histograms of inverted low frequency corner $\tau_1$ in the inner core for (a) global data and (b) North American data. Two dominant values of $\tau_1$ can be seen in both data sets. Almost no $\tau_1$ falls in the range of $10^1$ to $10^3$ s, which would be consistent with strong dispersion and frequency independent attenuation in the seismic band.

correlation between observed and predicted PKP-DF using RSTFs can be high (>95%) for many more stations in the distance range around 150° than the correlation obtained using PKP-BC as a reference waveform. Hence, the use of RSTFs cannot only extend the distance range in which inner core attenuation parameters can be measured, it can also increase the number of attenuation measurements in the distance range around 150° where PKP-BC can be observed.

[25] These tests do not address the problem associated with strong deviations from a radially symmetric attenuation structure in the mantle being mapped into PKP-DF, which the use of the PKP-BC reference waveform avoids. The greater volume of measurements possible with the use of RSTFs partially mitigates this problem when a sufficient number of measured paths exist through a region of the inner core that end at source and receivers lying above spatially separated regions of the mantle. Corrections for lateral variations in mantle attenuation structure, however, are still desirable when reliable values become available, and may eventually reduce the scatter in results.

## 4. Results: Intrinsic Attenuation

[26] Figure 11 shows the global distribution of ray turning points of PKIKP waveforms used in the inversion. The average $Q$ for the inner core determined from these paths is 307 with estimated error of ±90. This is consistent with the values given in previous studies [*Cormier*, 1981; *Choy and Cormier*, 1983; *Doornbos*, 1983].

### 4.1. Depth Dependence

[27] Figures 12a, 12b, and 12c show the variation of $Q^{-1}$ at 1 Hz as a function of radius and ray direction at the turning point of the PKIKP phase in the inner core, for global, North American, and East Asia data, respectively. The ray direction is quantified by the dot product of the tangent at the ray turning point with the direction of the Earth's spin axis. Although the data exhibit large scatter as in previous studies [e.g., *Bhattacharyya et al.*, 1993; *Souriau and Roudil*, 1995], the depth dependence and anisotropy of the inner core attenuation are clearly visible in Figures 12a–12c for both global and regional results. With increasing radius of the ray turning point (decreasing depth of inner core penetration), the attenuation increases, with especially high attenuation values at radii higher than 600 km (600 km is approximately the middle of the inner core). With PKIKP data in the distance range of 150° ∼ 180°, the corresponding radii of turning points will span almost all of the inner core from 0 to about 1000 km. With the large scatter typical of spectral ratios of narrow band short-period data, it is very difficult to resolve the depth dependence over the shorter range of depths sampled in previous studies [e.g., *Niazi and Johnson*, 1992; *Bhattacharyya et al.*, 1993; *Souriau and Roudil*, 1995].

### 4.2. Anisotropy

[28] Significant anisotropy of attenuation is visible in Figures 12a–12c. Rays traveling close to the equatorial plane tend to suffer small attenuation, while rays traveling close to the spin axis tend to suffer large attenuation. *Souriau and Romanowicz* [1996] found clear evidence of anisotropic attenuation in the inner core under West Africa from the analysis of the PKP-DF/PKP-BC amplitude ratios. Here, using waveform fitting in the time domain, two more regions, North America (Figure 12b) and East Asia (Figure 12c), are added to observations of attenuation anisotropy of the inner core.

[29] Why was it difficult for many previous studies to resolve the attenuation anisotropy? One reason may be due to sparse data, making the sampling in the inner core too scattered to provide constraints on attenuation as analyzed by *Souriau and Romanowicz* [1996]. Another reason could be due to the small depth interval considered in previous studies. Limited by the use of PKP-BC, most of the previous studies just focused on the upper most several hundred kilometers of the inner core. Recent research on elastic anisotropy [*Shearer*, 1994; *Su and Dziewonski*, 1995; *Song and Helmberger*, 1995; *Song*, 1996] have found that the anisotropy in the deep part of the inner core is stronger than that in the shallow part of inner core. These travel time studies suggest that the outermost 50 ∼ 200 km of inner core may not have *any* elastic anisotropy. Thus, it is understandable that previous studies could not find the anelastic anisotropy if, as in the case of elastic anisotropy, the anelastic anisotropy also exists primarily in the deeper part of the inner core.

[30] Because observations of elastic anisotropy find the fastest ray paths are close to the spin axis, it is expected that

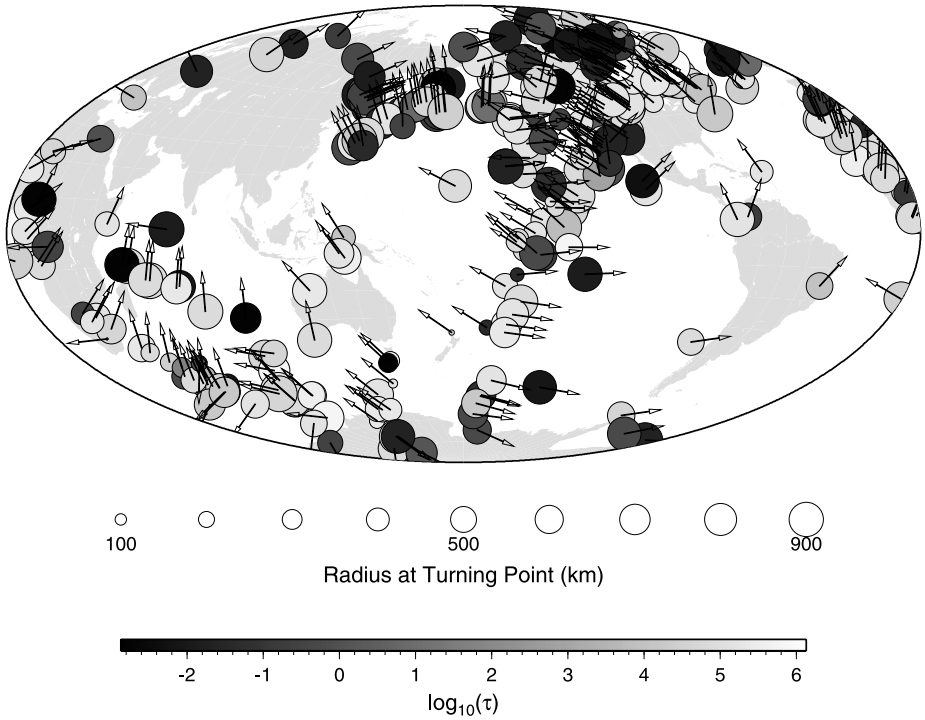


**Figure 18.** The gobal distribution of the inverted low frequency corner $\tau_1$ plotted at ray trning points. The arrow on each result indicates the ray direction at the turning point. Note that low and high $\tau_1$ coexist in nearly the same regions at nearly the same ray directions.

high attenuation should correlate with the faster traveling waves PKIKP observed along polar paths. The results of a global analysis, however, cannot systematically resolve this correlation (Figure 13a), even though the travel time residuals of our data show clear anisotropy (Figure 14) similar in magnitude to previous studies of elastic anisotropy [e.g., *Creager*, 1992; *Song and Helmberger*, 1993]. One reason why it may be difficult to resolve this correlation is that the

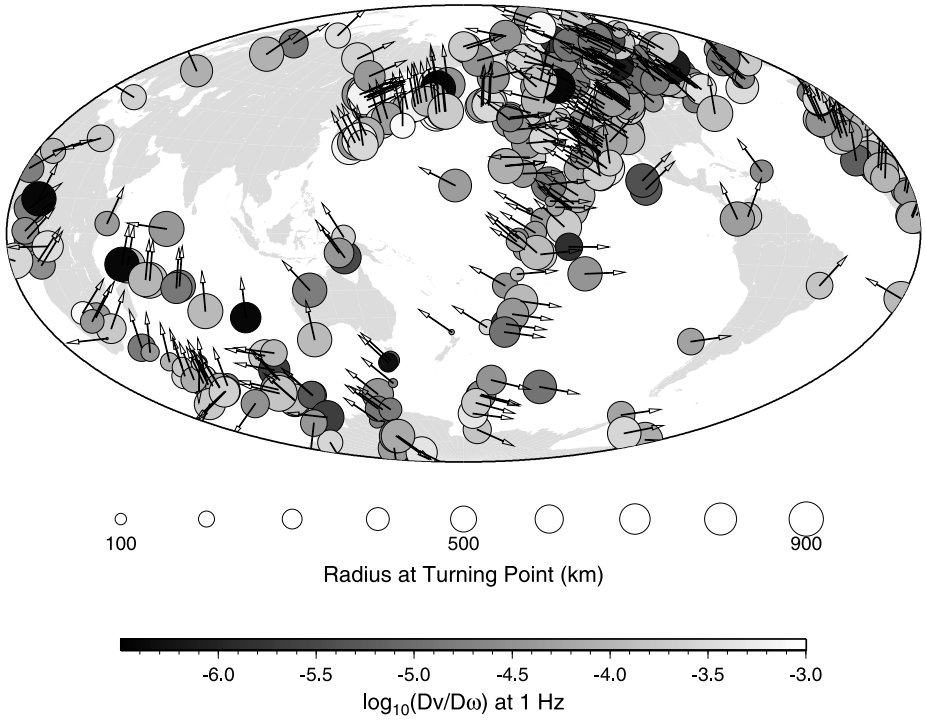


**Figure 19.** The gobal distribution of the velocity derivative with respect to frequency $d\alpha/d\omega$ at 1 Hz plotted at the ray turning points. The arrow on each result indicates the ray direction at the turning point.

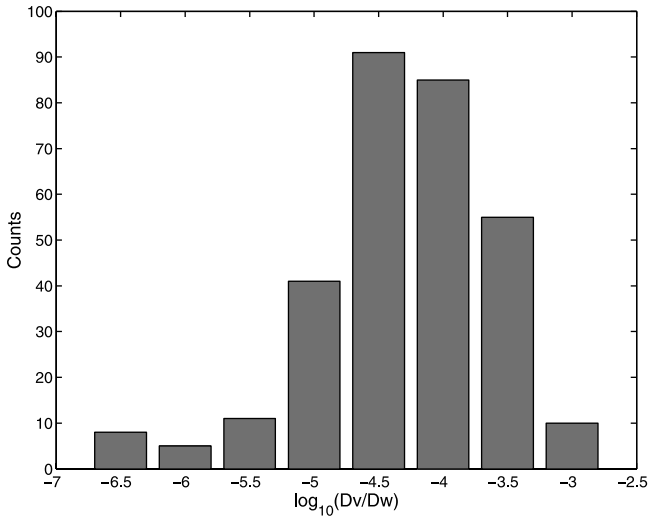


**Figure 20.** The histogram of the velocity derivative with respect to frequency, $d\alpha/d\omega$, at 1 Hz. Note that there is just one dominant value, consistent with very low dispersion in the body wave band.

variation of attenuation in the inner core is a function not only of ray direction, but also of depth and lateral location. The results of *Souriau and Romanowicz* [1996], which sampled only a small geographic region, may have overcome the effects of lateral heterogeneity of depth dependence that tend to cancel the signal due to orientation of ray path. If the analysis of travel time and attenuation correlation is confined to a localized region, as under North America and East Asia, then there is indeed some tendency of a correlation of high attenuation with fast velocity (Figures 13b and 13c).

### 4.3. Hemispheric Variation

[31] Some evidence of the lateral variation of attenuation and its depth dependence has been documented by *Niu and Wen* [2001], who find a significant difference in attenuation in the upper part of the inner core between the eastern and western hemispheres of the inner core. The hemispherical difference in attenuation correlates with variations in differential travel time PKiKP−PKIKP. In our study of the deeper inner core, we find that there are no obvious attenuation differences between the two hemispheres (Figure 15). This result could be due to two factors: (1) the hemispherical difference is too small to be discriminated from the strong depth dependence of attenuation; or (2) hemispherical differences are canceled by deep rays that penetrate across two hemispheres in which the attenuation difference is confined to just the top of the inner core. If the analysis of our data is confined to just the northern hemisphere, the attenuation beneath the eastern quarter sphere is greater than that beneath the western quarter sphere (see Figure 16). Anisotropy of attenuation, however, will also effect this observation. One way to investigate the possible hemispherical difference in the deep part of the inner core is to analyze the rays traveling only in polar directions beneath the eastern or western hemispheres. Unfortunately, our data set, containing no more than 10 of these kinds of rays, is too small to perform such an analysis.

### 4.4. Frequency Dependence

[32] The histograms of the results for low frequency corner $\tau_1$ for the global and North America data are given in Figure 17. It can be seen that $\tau_1$ in the inner core has two dominant values. One is around $10^5$ s and another is around $10^{-1}$ s. Both of them will imply a frequency-dependent attenuation in the seismic band. The former value predicts decreasing attenuation with frequency and latter one predicts increasing attenuation with frequency. Almost no data suggest a constant $Q$ in the frequency band of seismic body wave. In other words, the dispersion in the inner core is very weak. This observation is consistent with the studies of *Doornbos* [1983].

[33] A check of the global distribution of the inversion results for $\tau_1$ (Figure 18), shows that the low and high $\tau_1$ values are not spatially coherent, with both low and high values clustering in similar locations. This may signify a problem in the sensitivity to this parameter. The inverse method seeks an attenuation operator that gives the best waveform fit, which will depend on the frequency dependence of both real and imaginary parts of the complex velocity $\alpha(\omega)$. As shown in Figure 2, when $Q^{-1}(1\text{ Hz}) = 0.002 \sim 0.004$ and $\tau_1$ is near either $10^{-1}$ or $10^5$ s, the frequency dispersion of velocity will be very low and it will be hard to discriminate between the very small difference in velocity dispersion between these two different regions of the relaxation spectrum, which differ only in the second derivative of velocity with respect to frequency. Rather than the low or high frequency corner of the relaxation spectrum, a more robust parameter determined by the inversion is the first derivative of velocity with respect to frequency, $d\alpha/d\omega$, which can be similar in both the low and high frequency corners regions of the relaxation spectrum. Thus our data are consistent with a frequency band lying near either the low or high frequency corner. The global distribution of $d\alpha/d\omega$ displays a good spatial coherence (Figure 19). Only one dominant value of $d\alpha/d\omega$ occurs in a histogram of our results (Figure 20), and the values tend to obey a Gaussian distribution with a mean near $10^{-4.5} \sim 10^{-4}$ km. We thus conclude that the attenuation in the inner core is frequency dependent and the corresponding velocity dispersion with frequency in the inner core is very weak in the seismic body wave band.

## 5. Conclusions

[34] Using a viscoelastic model, this study has found evidence for depth-dependent and anisotropic attenuation in the inner core. The most significant result, which we feel has the deepest implications for the physical mechanism of attenuation, is the relatively weak dispersion required to fit observed waveforms. This result agrees with earlier observations of *Doornbos* [1983] and *Cummins and Johnson* [1988]. The weak dispersion can be fit by viscoelastic models that have either the low or high frequency corner of the relaxation spectrum lying near or within the frequency band of short period body waves. Weak pulse dispersion, or at least weaker than that predicted by a viscoelastic model for band of frequency independent attenuation, is a well known characteristic of scattering [*Richards and Menke*, 1983]. Paper 2 of this study investigates the possibility that it is forward scattering by small-

scale heterogeneity rather than viscoelasticity that broadens pulse widths in the body wave band.

[35] **Acknowledgments.** This research was supported by grant EAR 99-80355 from the National Science Foundation. We thank Michael Bergman, Paul Earle, Lane Johnson, and John Vidale for preprints and helpful discussions, and two anonymous reviewers.

## References

Anderson, D. L., and J. W. Given, Absorption band Q model for the Earth, *J. Geophys. Res.*, *87*, 3893–3904, 1982.

Barker, J. S., and C. A. Langston, Moment tensor inversion of complex earthquakes, *Geophys. J.*, *68*, 777–803, 1982.

Barker, J. S., and C. A. Langston, A teleseismic body-wave analysis of the May 1980 Mammoth Lakes, California earthquakes, *Bull. Seismol. Soc. Am.*, *73*, 419–434, 1983.

Bhattacharyya, J., P. M. Shearer, and G. Masters, Inner core attenuation from short-period PKP (BC) versus PKP (DF) waveforms, *Geophys. J. Int.*, *114*, 1–11, 1993.

Carcione, J. M., and F. Cavallini, A rheological model for anelastic anisotropic media with application to seismic wave propagation, *Geophys. J. Int.*, *119*, 338–348, 1994.

Chin, R. C., Wave propagation in viscoelastic media, *Phys. Earth Planet. Inter.*, *78*, 213–246, 1980.

Choy, G. L., and V. F. Cormier, The structure of the inner core inferred from the short period and broadband GDSN data, *Geophys. J. R. Astron. Soc.*, *72*, 1–21, 1983.

Cormier, V. F., Short-period PKP phase and the anelastic mechanism of the inner core, *Phys. Earth Planet. Inter.*, *24*, 291–301, 1981.

Cormier, V. F., and P. G. Richards, Spectral synthesis of body waves in Earth models specified by vertically varying layers, in *Seismological Algorithms*, pp. 1–45, Academic, San Diego, Calif., 1988.

Cormier, V. F., X. Li, and G. L. Choy, Seismic attenuation of the inner core: Viscoelastic or stratigraphic?, *Geophys. Res. Lett.*, *25*, 4019–4022, 1998.

Creager, K. C., Anisotropy of the inner core from differential travel times of the phases PKP and PKIKP, *Nature*, *356*, 309–314, 1992.

Cummins, P., and L. R. Johnson, Short-period body wave constraints on properties of the Earth's Inner Core Boundary, *J. Geophys. Res.*, *93*, 9058–9074, 1988.

Doornbos, J. D., Observable effects of the seismic absorption band in the Earth, *Geophys. J. R. Astron. Soc.*, *75*, 693–711, 1983.

Dziewonski, A. M., and D. L. Anderson, Preliminary reference Earth model, *Phys. Earth Planet. Inter.*, *25*, 297–356, 1981.

Fearn, D. R., D. E. Loper, and P. H. Roberts, Structure of the Earth's inner core, *Nature*, *292*, 232–233, 1981.

Jackson, I., J. D. Fitzgerald, and H. Kokkonen, High-temperature viscoelastic relaxation in iron and its implications for the shear modulus and attenuation of the Earth's inner core, *J. Geophys. Res.*, *105*, 23,605–23,634, 2000.

Langston, C. A., and D. V. Helmberger, A procedure for modeling shallow dislocation sources, *Geophys. J. R. Astron. Soc.*, *42*, 117–130, 1975.

Liu, H. P., D. L. Anderson, and H. Kanamori, Velocity dispersion due to anelasticity; implications for seismology and mantle composition, *Geophys. J. R. Astron. Soc.*, *47*, 41–58, 1976.

Lundquist, G. M., and V. F. Cormier, Constraints on the absorption band model of Q, *J. Geophys. Res.*, *85*, 5244–5256, 1980.

Minster, J. B., Transient and impulse responses of a one-dimensional linearly attenuating medium, 1, Analytical results, *Geophys. J. R. Astron. Soc.*, *52*, 479–502, 1978a.

Minster, J. B., Transient and impulse responses of a one-dimensional linearly attenuating medium, 2, A parametric study, *Geophys. J. R. Astron. Soc.*, *52*, 503–523, 1978b.

Minster, J. B., Anelasticity and attenuation, *Phys. Earth Inter.*, *78*, 152–212, 1980.

Niu, F. L., and L. X. Wen, Hemispherical variations in seismic velocity at the top of the Earth's inner core, *Nature*, *410*, 1081–1084, 2001.

Niazi, M., and L. R. Johnson, Q in the inner core, *Phys. Earth Planet. Inter.*, *74*, 55–62, 1992.

O'Connell, R. J., Grain boundary relaxation in the mantle, *Eos Trans. AGU*, *59*, 1183, 1978.

Richards, P. G., and W. Menke, The apparent attenuation of a scattering medium, *Bull. Seismol. Soc. Am.*, *73*, 1005–1021, 1983.

Sacks, I. S., Anelasticity of the inner core, *Year Book Carnegie Inst. Washington*, *69*, 416–419, 1969.

Shearer, P. M., Constraints on the inner core anistropy from PKP(DF) travel times, *J. Geophys. Res.*, *99*, 19,647–19,659, 1994.

Song, X. D., Anisotropy in the central part of the inner core, *J. Geophys. Res.*, *101*, 16,089–16,097, 1996.

Song, X. D., and D. V. Helmberger, Anisotropy of the Earth's inner core, *Geophys. Res. Lett.*, *20*, 2581–2594, 1993.

Song, X. D., and D. V. Helmberger, Depth dependence of anisotropy of Earth's inner core, *J. Geophys. Res.*, *100*, 9805–9816, 1995.

Souriau, A., and B. Romanowicz, Anisotropy in the inner core attenuation: A new type of data to constrain the nature of the solid core, *Geophys. Res. Lett.*, *23*, 1–4, 1996.

Souriau, A., and P. Roudil, Attenuation in the upper most inner core from broadband Geoscope PKP data, *Geophys. J. Int.*, *123*, 572–587, 1995.

Steinle-Neumann, G., L. Stixrude, R. E. Cohen, and O. Gulseren, Elasticity of iron at the temperature of the Earth's inner core, *Nature*, *413*, 57–60, 2001.

Su, W. J., and A. M. Dziewonski, Inner core anisotropy in the three dimensions, *J. Geophys. Res.*, *100*, 9831–9852, 1995.

Tarantola, A., *Inverse Problem Theory*, 613 pp., Elsevier Sci., New York, 1987.

Widmer, R., G. Masters, and F. Gilbert, Spherically symmetric attenuation within the Earth from normal mode data, *Geophys. J. Int.*, *104*, 541–553, 1991.

V. F. Cormier, Department of Geology and Geophysics, University of Connecticut, Room 207, 354 Mansfield Road, Storrs, CT 06269-2045, USA. (cormier@geol.uconn.edu)

X. Li, Earth Resources Laboratory, Department of Earth, Atmospheric, and Planetary Science, Massachusetts Institute of Technology, 42 Carleton Street, Cambridge, MA 02142, USA. (xuli@erl.mit.edu)